NUMERICAL STUDIES ON SPIN COATING OF METALS

by

VARUN NANJUNDA RAO VISWAMITHRA

Presented to the Faculty of the Graduate School of
The University of Texas at Arlington in Partial Fulfillment
of the Requirements
for the Degree of

Master of Science in Mechanical Engineering

THE UNIVERSITY OF TEXAS AT ARLINGTON
April 2016

ACKNOWLEDGEMENTS

Firstly, I would like to express my sincere gratitude to my research advisor Dr. Albert Y. Tong for the continuous support of my M.S. thesis study and related research, for his patience, motivation, and immense knowledge. His guidance helped me in all the time of research and writing of this thesis.

I would also like to thank the rest of my thesis committee: Dr. Ankur Jain and Dr. Ratan Kumar and for their insightful comments and encouragement which incented me to widen my research from various perspectives.

A special thanks to Vimal Ramanuj for helping me in multiple ways during the course of my research. I thank my fellow teammates Alex Yuan, Davis, Peter Martinez and Vimalan for the stimulating discussions and for all the fun we have had in the last two years. Also I thank my friends Abhishek, Aishwarya, Ashwin, Harshitha, Nayana, Rakesh, Shashank, Varsha, Vijay and Vivekananda for their valuable inputs.

Last but not the least, I would like to thank my family: my parents R.Vijayalakshmi and L. R. Nanjunda Rao, my brother Vineeth for suporting me spiritually throughout writing this thesis and my life in general.

April 14, 2016

ABSTRACT

NUMERICAL STUDIES ON SPIN COATING OF METALS

Varun Nanjunda Rao Viswamithra, M.S

The University of Texas at Arlington, 2016

Supervising Professor: Dr. Albert Y. Tong

Spin coating is a surface coating process which involves spreading a liquid dispensed on the center of a rotating substrate. The liquid is discharged using a suitable method on to the substrate rotating at a constant angular speed. The spinning speed is controlled to obtain a coating of desired thickness with faster spinning resulting in thinner coating. The thickness of the coating also depends on the properties of the fluid and other process parameters.

Centrifugal force is introduced into the code as radial component of acceleration. The first part of the code solves the continuity and the Navier-Stokes equations, with which the pressure and velocities are obtained. Solution to the Navier-Stokes is obtained using the two-step projection method. An intermediate velocity is generated in the first step which is used in the second step when a pressure poison equation (PPE) is solved with the value of the intermediate velocity obtained from the first step. In the second part of the code, free surface tracking is done using a Coupled Level Set Volume of Fluid (CLSVOF) method. In CLSVOF method, the combined advantage of Volume of Fluid (VOF) and

Level Set (LS) results in efficient mass conservation and accurate free surface reconstruction. Solidification is done using an enthalpy-porosity technique with a source term accounting for phase change.

In this study, thin film formation under the action of spinning is investigated. A parametric study is carried out. The effects of angular velocity, ramp rate, substrate temperature, initial droplet temperature and latent heat on the thickness of coating are studied. The results obtained are in accordance with experimental data reported in the literature.

TABLE OF CONTENTS

LIST OF ILLUSTRATIONS

CHAPTER 1

Introduction

Coating is a covering that is applied to the surface of an object. The object is generally referred to as substrate. Coating can be applied to whole surface or part of the surface. An example of coating is the that of a compact disc (CD), where a thin layer of coating is used to store data.

Paints and lacquers are coatings have dual uses of protecting the substrate and being decorative, although some artists paints are only for decoration. The paint on large industrial pipes is presumably only for the function of preventing corrosion.

Functional coatings are applied to change the surface properties of the substrate such as adhesion, wettability, corrosion. The coating imparts a new property in the fabrication of semiconductor devices. The properties include magnetic response, conductivity and forms an integral of the finished product.

A major consideration for most coating processes is that the coating is to be applied at a controlled thickness, and a number of different processes are in use to achieve this control. Few such methods are spray coating, spin coating, dip coating.

Many industrial coating processes involve the application of a thin film of functional material to a substrate. A thin film is a layer of material ranging from fractions of a nanometer (mono-layer) to several micrometers in thickness. Electronic semiconductor devices and optical coatings are the main applications benefiting from thin-film applications. A familiar application of thin films is the

household mirror, which typically has a thin metal coating on the back of a sheet of glass to form a reflective interface.

The performance of optical coatings are typically enhanced when the thin-film coating consists of multiple layers having varying thicknesses and refractive indices. Work is being done with ferromagnetic and ferroelectric thin films for use as computer memory. It is also being applied to pharmaceuticals, via thin-film drug delivery. Thin-films are used to produce batteries and solar cells.

Ceramic thin films are in wide use. The relatively high hardness and inertness of ceramic materials make this type of thin coating of interest for protection of substrate materials against corrosion, oxidation and wear. In particular, the use of such coatings on cutting tools can extend the life of these items by several orders of magnitude.

The physics of spin coating are modeled by dividing the process into four successive stages.

The key stages involved in spin coating process are:

- Deposition
- Spin-up
- Spin-off/Stable fluid flow and
- Evaporation.

Deposition: During this stage, solution is allowed to fall on rotating substrate using a suitable discharge mechanism. The substrate is accelerated to the desired speed. Spreading of the solution takes place due to centrifugal force.

Spin-up: The substrate in this stage is accelerated up to its maximum desired rotation speed. In this stage fluid moves radially outwards over the wafer due to rotational motion. The fluid is thin enough that the viscous shear drag exactly balances the rotational accelerations.

Spin-off/Stable fluid flow: In this stage fluid thinning is quite uniform. Edge effects are often seen because the fluid flows uniformly outward, but form droplets at the edge to be flung off. Thus depending on surface tension, viscosity, rotation rate, mathematical representation of the flow shows that if the liquid exhibits Newtonian viscosity and if the fluid thickness is uniform initially, the fluid thickness profile at any point at any following time will also be uniform.

Evaporation: If a polymeric photo-resist material is used, it is generally dissolved in solvent. The solution is dispensed and after spinning the substrate is heated to a temperature sufficient to remove the solvent by means of evaporation. Figure below summarizes the spin coating process.

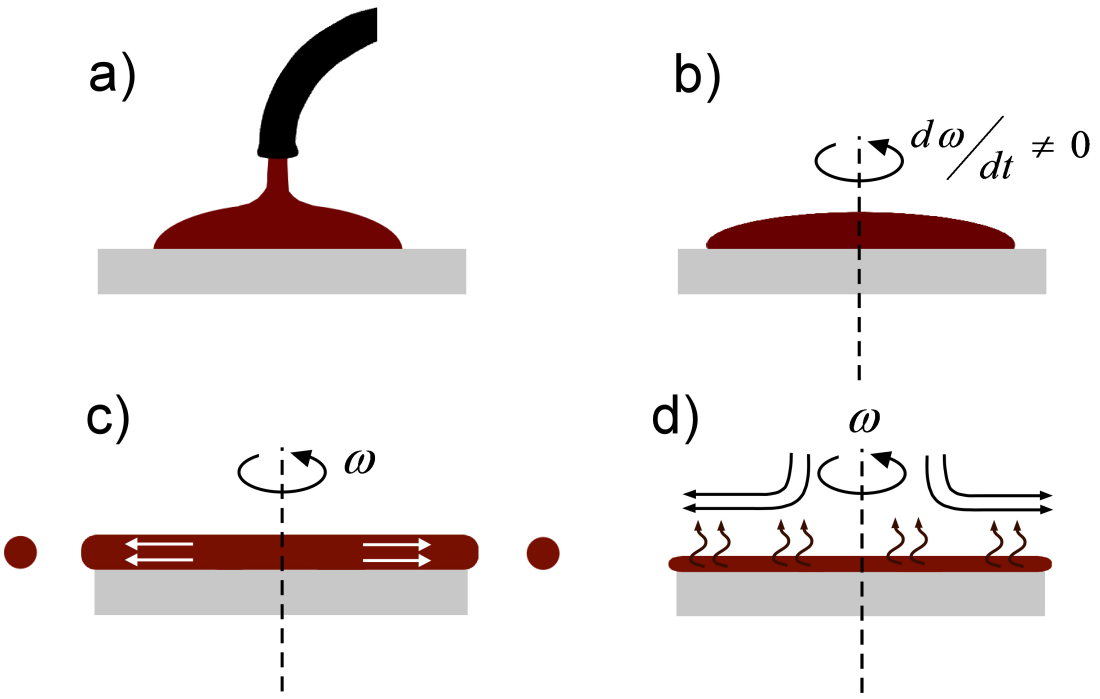

Figure 1.1: Key stages in spin coating process

CHAPTER 2

Literature Review

Spin Coating process has been of interest to many researchers. A variety of photo-resists materials has synthesized over time. It is a predominant technique employed to produce uniform thin films with thickness of the order of the micrometers and nanometers. First ever analysis on spin coating was done 50 years ago by A.G. Emslie, F.T. Bonner and L.G. Peck [3]. The analysis considered spreading of thin axis-symmetric film of Newtonian fluid on a flat substrate rotating at a constant angular velocity.

In most cases the material used is polymeric. The polymer is generally dissolved in a suitable solvent. The solution so prepared is dispensed on the substrate and is made to spin giving rise to a thin film. Properties of photo-resists play key role in the end product to be developed. A large group of properties possessed by the resist play a key role in establishing its functionality. They are optical properties like resolution,photo-sensitivity and refractive index. Mechanical properties such as viscosity, adhesion, etch, resistance, thermal stability, flow characteristics and sensitivity to ambient gases. Processing and safety related properties including cleanliness, process latitude, shelf life.

2.1 Experimental Technique:

The bulk of semiconductors fabricated today have resist critical dimensions above 250 nm; this is also true of MEMS technology, GaAs, InP, LiNbO3, and other substrate-type technologies. For feature sizes of this magnitude and larger,

positive i-line resist is the optimal lithographic film; i-line resists mainly consist of three components: resin, solvent, and PAC (photo-active compound).

Many substrates may be coated, but in many research applications one-inch square glass plates (for many applications often coated with a transparent electrode made of indium tin oxide or ITO) cut from microscope slides are commonly coated for experimental purposes. Prior to spin-coating, the polymer-solvent solution must be filtered to remove dust, typically with a 0.45 micrometer filter. Although it is preferable to spin-coat in a clean-room environment (Class 10 or 100), for many simple laboratory experiments, spin-coating may be performed in a clean fume-hood. The glass plate is placed upon the spin-coating apparatus, cleaned successively with acetone and then methanol using lint-free swabs, and followed up with isopropanol, then coated liberally with the polymer-solvent solution by use of syringe or eye-dropper. The plate is spun in at least two stages which may be programmed into most any simple spin-coating apparatus. During the first stage, the plate is spun at a low to moderate speed 500 to 1000 rpm for a duration of 5 to 10 seconds to evenly spread the solution. The thickness of the coating is then determined and controlled during the second stage by spinning the coating at a higher speed, between 1500 to 3000 rpm for anywhere between a few seconds and a minute. These conditions will typically produce high quality coatings of thickness between 2 and 10 micrometers.

2.2 Key Process Parameters:

2.2.1 Spin Speed:

Spin Speed is one of the most important factors in spin coating process. The speed of the substrate affects the degree of radial (centrifugal) force applied.

In particular, high speed spin generally defines the final thickness achieved on the substrate. Relatively minor variations of ±50 rpm at this stage can cause a resulting thickness change of 10%. Film thickness is largely a balance between force applied to shear the liquid film towards the edge of the substrate and cooling rate which affects the viscosity of the liquid film. As film cools down the viscosity increases until the radial force due to spinning action can no longer appreciably move over the substrate.

2.2.2 Acceleration:

The acceleration of the substrate towards the final spin speed can also affect the film properties. Since the liquid film begins to cool in the first part of the spin cycle. It is important to accurately control acceleration. Acceleration plays a key role in the coat properties of the patterned substrates. In many cases substrates will retain topographical features from previous processes it is therefore important to uniformly coat the liquid film over and through these features while the spin process in general provides a radial outward force to liquid film.

2.2.3 Viscosity:

Viscosity plays an important role in the spin coating process. It is physical property of the liquid film being coated. The higher the viscosity of the liquid, higher spin speeds are needed to have the liquid spread. Lower the viscosity lower spin speeds are sufficient to have an even spread over the substrate. Viscosity indirectly controls the total time required for the process to reach completion.

2.3 Mathematical Description:

Mathematical treatment of the spin coating process is essential to simulate it on a computer. The treatment is based on assuming that flow has reached a stable condition where the centrifugal and viscous forces are just in balance. The force balance equation is :

$$-\eta \frac{\partial^2 \nu}{\partial z^2} = \rho \omega^2 r \tag{2.1}$$

where z and r define a cylindrical coordinate system aligned with axis of substrate rotation, ν is the fluid velocity in the radial direction, r is perpendicular distance from the axis of rotation, ρ is the fluid density, η is the fluid viscosity, ω is the angular velocity of the substrate, it is worth mentioning here that as we move away from the axis of rotation the force experienced by the liquid increases.
with appropriate flow and velocity boundary conditions and considering the film to be uniform initially, the film thickness as a function of time h(t), is found to be:

$$h = \frac{h_0}{\sqrt{1 + 4Kh_0^2 t}} \tag{2.2}$$

where h_0 is the film thickness at time zero. and K is a system constant defined as:

$$K = \frac{\rho \omega^2}{3\eta} \tag{2.3}$$

These equations are strictly valid only when K is constant. However for spin coating of sol-gel or other complex solutions this many not hold true during all stages of spinning. Detailed description of the mathematical formulation can be found in [4, 5].

2.4 Motivation

The mathematical model discussed in [4, 5], addresses the spin coating without taking into account the unsteady effects during the initial stages of the process. The study does not account for the non-linearity present in the process. This led to the numerical studies on the same. The current model can address the transient nature of the problem and does account for the non-linearity. Tin is used in the present study. The reason for having chosen tin for this study is because, tin is used for coating of films. It is done so by means of spray coating. Spin coating in most cases is a process carried out on Non-Newtonian fluids. There was no data available with reference to spin coating carried out by making use of tin. This study attempts to model the process with the use of molten metal (tin) which is Newtonian.

CHAPTER 3

Numerical Formulation

There are three important steps in the computational modeling of any physical process: (a) problem definition, (b) mathematical model, and (c) computer simulation.

The first step is to define our problem of interest in terms of a set of relevant quantities which are of our interest. In defining the idealization we expect to obtain a well-posed problem, one that has a unique solution for a given set of parameters. It might not always be possible to guarantee the dependability of the idealization since, in some instances, the physical process is not completely understood.

The next step of the modeling process is to represent our idealization of the physical phenomenon by a mathematical model: the governing equations of the problem. In fluid dynamics, the continuity and the Navier-Stokes equations are considered to be an accurate representation of the fluid motion. Equations of elasticity in structural mechanics govern the deformation of a solid object due to the application of external forces. The general equations are very difficult to solve both analytically and computationally. Therefore, it is necessary to introduce assumptions to reduce the complexity of the mathematical model.

After the selection of appropriate mathematical model, and in conjunction with suitable boundary and initial conditions, we can proceed to solve the equations by making use of solution schemes. The three choices for the numerical solution of PDEs are the Finite Difference Method (FDM), the Finite Element

Method (FEM) and the Finite Volume Method (FVM). The FDM uses a topologically square network of lines to construct the discretization of the PDE. There is a difficulty associated with the use of this method when handling complex geometries in multiple dimensions. This encouraged the use of an integral form of the PDEs and subsequently the development of the finite element and volume techniques. Application of computational studies to spin coating process helps us in analyzing various parameters such as flow field. These data extracted helps us in reducing material wastage, minimize the contact with dangerous fumes. Spin coating is a very popular process in electronic fabrication industry.

It is necessary to track the free surface as the problem under consideration is a moving boundary type problem. In the upcoming section we will discuss two important techniques used for free surface tracking. They are Coupled Level Set and Volume Of Fluid (CLSVOF) and Volume Of Fluid (VOF) methods.

Numerical analysis and simulation are widely used in engineering applications today because of the advantages over experimental and analytical solutions. Nonetheless we need experimental data to validate the numerical studies. There is a great deal of advantage that comes with the use of numerical analysis as it is a highly efficient method to carryout parametric studies, elementary design and calculations. Numerical analysis also serves as a means to carryout failure analysis. Details of the numerical formulation can be obtained from [1, 6, 7, 8].

The code used is a two dimensional, incompressible, laminar flow developed by Los Alamos National Lab (LANL) [6]. This code along with few modifications is made use of in our study of spin coating process. The protocol has two steps involved in the process. First is to solve the governing equations and second is to track the free surface. The code uses finite volume scheme on a fixed uniform grid to solve the governing equations and it uses VOF/CLSVOF to track the free

surface.

The second part of the simulation is the solidification of the liquid metal. An algorithm has been integrated in to the original code to handle the phase change process. An enthalpy based method is adopted to do so. In this method enthalpy-based formulation of the energy formulation of the energy equation which includes both convection-diffusion heat transfer and mushy-region for the phase change has been developed and has been embedded into the original code. The details of the formulation is discussed in the subsequent sections.

3.1 Governing Equations

Flow of the liquid droplet is assumed to be incompressible and is governed by continuity and Navier-Stokes equations given by:

$$\nabla \cdot \vec{V} = 0 \tag{3.1}$$

$$\frac{\partial \vec{V}}{\partial t} + \nabla \cdot (\vec{V}\vec{V}) = -\frac{1}{\rho}\nabla P + \frac{1}{\rho}\nabla \tau + \vec{g} + \frac{1}{\rho}\vec{F_b} \tag{3.2}$$

where ρ is the density, P is the scalar pressure, τ the viscous stress tensor, $\vec{F_b}$ a body force and $\vec{g}$ is the acceleration due to gravity. The nonlinear advection term is written in conservative form. The viscous stress tensor τ is Newtonian,

$$\tau = 2\mu S \tag{3.3}$$

$$S = \frac{1}{2}[(\nabla \vec{V}) + (\nabla \vec{V})^T] \tag{3.4}$$

where S is the rate of strain tensor and μ is the coefficient of dynamic viscosity. Viscous velocity boundary conditions at any rigid walls present in the domain are enforced as either no slip where,

$$\vec{V} = 0, \tag{3.5}$$

at the wall, or free-slip where $\hat{n}_w \cdot \vec{V} = 0$, $\hat{n}_w$ being the unit normal to the wall.

The governing equation is a partial differential equation which is dependent on both time and spatial coordinates. Hence it needs to be discretized in time as shown below:

$$\frac{\vec{V}^{n+1} - \vec{V}^n}{\delta t} = -\nabla \cdot (\vec{V}\vec{V})^n - \frac{1}{\rho^n}\nabla p^{n+1} + \frac{1}{\rho^n}\nabla \cdot \tau^n + \vec{g}^n + \frac{1}{\rho^n}\vec{F_b}^n \tag{3.6}$$

where the superscripts n and n+1 represents the value of the variable at consecutive time steps. The only implicit term in the above equation is the pressure gradient. Gravity advection, surface tension and viscosity are approximated with old time t^n values. A two step projection method is used to separate the above equation into two as:

$$\frac{\vec{\tilde{V}} - \vec{V}^n}{\delta t} = -\nabla \cdot (\vec{V}\vec{V})^n + \frac{1}{\rho^n}\nabla \cdot \tau^n + \vec{g}^n + \frac{1}{\rho^n}\vec{F_b}^n \tag{3.7}$$

$$\frac{\vec{V}^{n+1} - \vec{\tilde{V}}}{\delta t} = -\frac{1}{\rho^n}\nabla p^{n+1} \tag{3.8}$$

An intermediate velocity $\vec{\tilde{V}}$ between n and n+1 time step is considered. The initial change in velocity is due to advection, surface tension, gravity and viscosity which are all explicitly known. The change comes from the pressure gradient, which is implicit. Thus there are two steps involved in solving this governing equation. The first step requires finite difference expressions for the momentum advection and viscosity terms in Eq.(3.7). The second step requires a solution of a poisson equation for the pressure field Eq.(3.8). It is done so by projecting the velocity field onto a zero-divergence vector field. The two equations in the second step can be combined to into a single Poisson equation for pressure.

$$\nabla \cdot [\frac{1}{\rho^n}\nabla p^{n+1}] = \frac{\nabla \cdot \vec{\tilde{V}}}{\delta t} \tag{3.9}$$

The above equation can be solved by incomplete cholesky conjugate gradient method [9] to obtain the pressure and hence the velocity field for subsequent time steps.

3.2 Free Surface and its tracking methods

Free surface of a fluid is subject to both zero perpendicular normal stress and parallel shear stress, such as the boundary between two homogeneous fluids, for example liquid water and the air in the Earth's atmosphere. Unlike liquids, gases cannot form a free surface on their own.

The tracking of free surface in the spin coating process is a challenge as it is classified under moving boundary problems. It becomes difficult to accurately locate and model the free surface or an interface it if undergoes drastic changes in the displacement of the fluid during the flow. There are certain techniques developed to accomplish the same. They are broadly classified as Lagrangian methods and Eulerian methods [10]. Lagrangian methods track the interface explicitly by treating the interface points as particles and exact location of the interface is obtained directly by solving the equations of motion if these particles. Some of the Lagrangian based methods are moving grid, front tracking, boundary integral and particle-based methods. In case of Eulerian methods, the interface is represented by an appropriate field function, which is advected in time while solving the governing equations. The interface is then reconstructed depending on the properties and behavior of the field function. This category includes continuum advection, volume tracking, level set and phase field methods. The algorithm used for this study uses Eulerian approach. It uses both Volume of fluid and Level set methods to accurately tracking the free surface. Hence it is called Coupled

Level Set and Volume Of Fluid (CLSVOF) method. A Piecewise Linear Interface Construction(PLIC) is used to construct the free surface.

3.2.1 Volume of Fluid (VOF) method

Free surfaces in the code are represented with discrete Volume-Of-Fluid (VOF) data on the mesh. The VOF method is a powerful tool that enables a finite difference representation of free surface and interfaces that are arbitrarily oriented with respect to computational grid. This technique was developed from Marker and Cell (MAC) technique. MAC was developed by Francis Harrow and the Los Alamos National Laboratory [11]. In VOF technique, an exact representation of the free surface is not retained. Characteristic marker data (the VOF function), advected as a Lagrangian invariant, is the only available free surface information. If the free surface location is needed, an approximate reconstruction is of the free surface is performed from VOF data. The reconstructed free surface is not necessarily continuous, instead represented as a set of discrete, discontinuous line segments. A similar concept was used in the VOF method [12] that was developed in 1976. In this method the markers were replaced by scalar function F(x,y,z,t) which denotes the fraction of the cell which is occupied by fluid. Function F is essentially the ratio of the of fluid to the volume of cell. Following interpretation about a particular cell can be made from the corresponding value of VOF function 'F'.

$$\text{F (x,y,z,t)} \begin{cases} = 0, \text{ Cell is in the void region} \\ 0 < F < 1, \text{ Cell is at the interface} \\ = 1, \text{ Cell is in the fluid} \end{cases}$$

An example for the VOF functions representing a circular fluid element is

shown in Figure(3.1). The number in each cell denotes the volume fraction occupied by the liquid. The VOF functions are advanced by the following propagating equation.

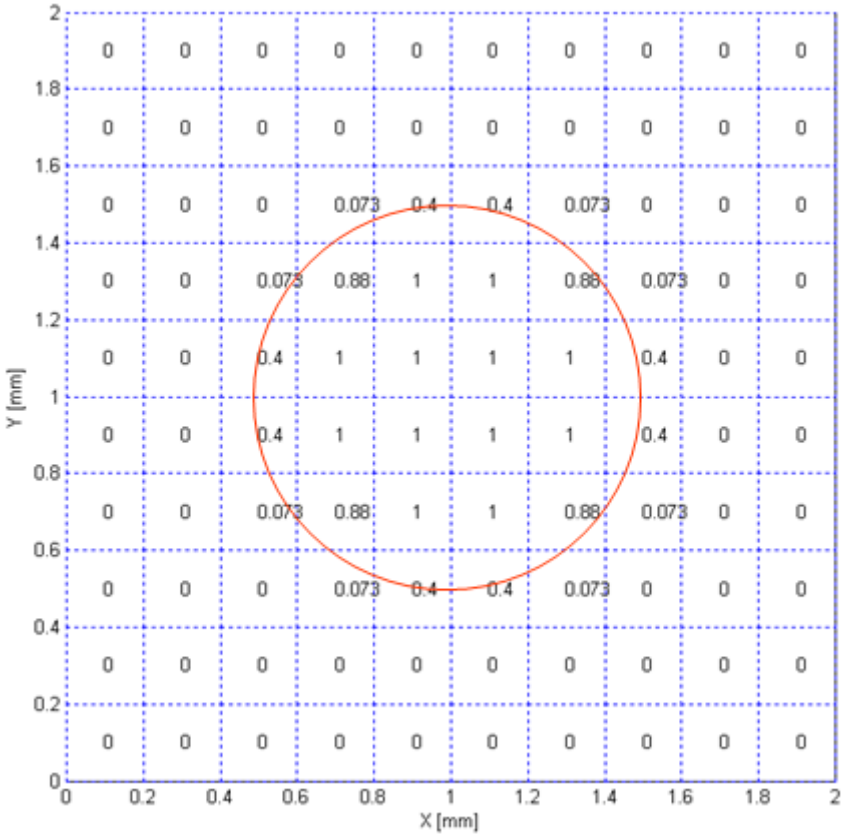

Figure 3.1: Volume of fluid function for a circular fluid element

$$\frac{D}{Dt}(F) = 0 \tag{3.10}$$

The above equation can be used in the conservative form to ensure mass conservation for all cells including the interface cells as follows:

$$\frac{\partial F}{\partial t} + \nabla \cdot (\vec{V}F) = F(\nabla \cdot \vec{V}) \tag{3.11}$$

It is discretized in time using an approach similar to one used for solving the governing equations.

$$\frac{\tilde{F} - F^n}{\delta t} + \frac{\partial}{\partial x}(uF^n) = \tilde{F}\frac{\partial u}{\partial x} \tag{3.12}$$

$$\frac{\vec{F}^{n+1} - \tilde{F}}{\delta t} + \frac{\partial}{\partial y}(v\tilde{F}) = F^{n+1}\frac{\partial v}{\partial y} \tag{3.13}$$

where $\tilde{F}$ is the intermediate VOF function. On the staggered grid, the VOF function, F, is located at the cell center and velocities, u and v are stored at the cell edges, as shown in Figure(3.2). Discretization of the above equations spatially and integrating over a computational cell(i,j) yields:

$$\tilde{F}_{i,j} = \frac{F^n_{i,j}\delta x_i \delta y_j - \delta t \delta y_j (flux_{i+\frac{1}{2},j} - flux_{i-\frac{1}{2},j})}{\delta x_i \delta y_j - \delta t \delta y_j (u_{i+\frac{1}{2},j} - u_{i-\frac{1}{2},j})} \tag{3.14}$$

$$F^{n+1}_{i,j} = \frac{\tilde{F}_{i,j}\delta x_i \delta y_j - \delta t \delta x_i (flux_{i,j+\frac{1}{2}} - flux_{i,j-\frac{1}{2}})}{\delta x_i \delta y_j - \delta t \delta x_i (v_{i,j+\frac{1}{2}} - v_{i,j-\frac{1}{2}})} \tag{3.15}$$

where $flux_{i\pm1/2,j} = (uF^n)_{i\pm1/2,j}$ and $flux_{i,j\pm1/2} = (v\tilde{F})_{i,j\pm1/2}$. They denote VOF fluxes across the edges of the computational cell. The calculation of the fluxes at the cell edges requires an interpolation scheme for the VOF functions which is described later. One important point worth noting about the VOF scheme is that it is only calculates the values of F and does not give any information about the orientation of the free surfaces or the interface. Generating an interface from the VOF data alone would result into discontinuities between neighboring cells. The circular profile shown in Figure(3.1) cannot be obtained from VOF data alone. VOF scheme is highly accurate in locating the free surface and conserving the mass in each cell but fails to identify the orientation of the free surface.

3.2.2 Level Set (LS) method

This method was developed by James Sethian and Stanley Osher [13, 14] during the late 1980's. The level set function ψ is defined as signed function whose

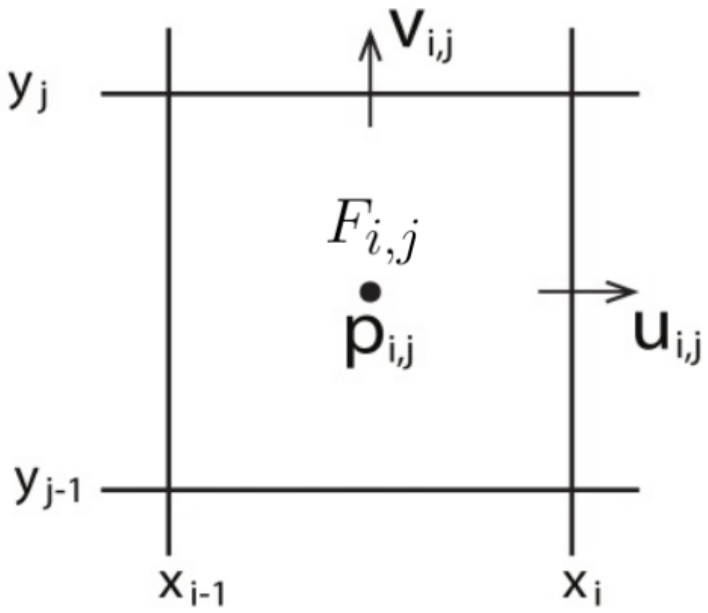

Figure 3.2: Staggered grid.

magnitude is equal to shortest distance of cell center from the interface or free surface. Following information can be drawn from the level set function.

$$\psi(x,y,z,t) \begin{cases} > 0, \text{ Cell center is outside of the fluid} \\ = 0, \text{ Cell center is at the interface} \\ < 0, \text{ Cell center is inside the fluid} \end{cases}$$

Following example in Figure(3.3) shows the use of Level Set function for a circular fluid element. The positive values indicate that the cell center is outside the fluid element while negative values indicate that it falls within the fluid.

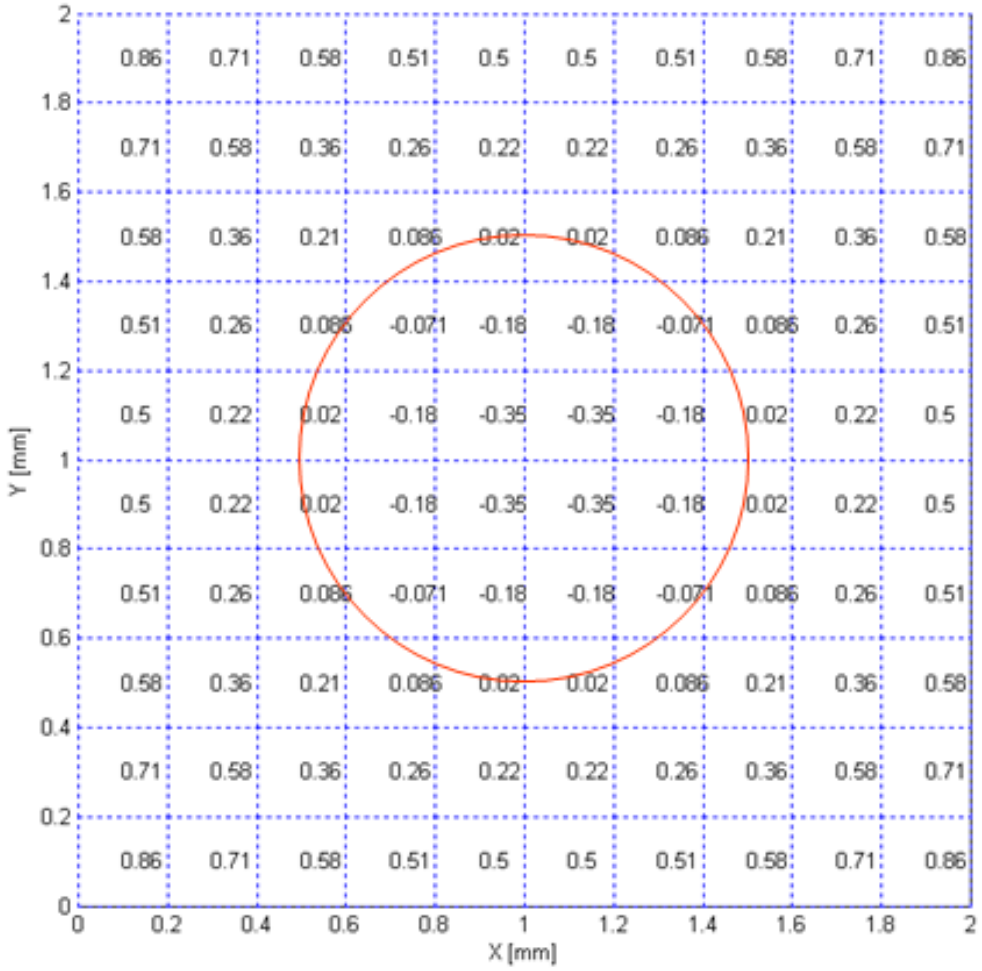

Figure 3.3: Level set function for a circular fluid element.

Another important property is that gradient of the level set function which gives a unit vector normal to the interface. Thus,

$$\vec{n} = \frac{\nabla\phi}{|\nabla\phi|} = \nabla\phi \tag{3.16}$$

$$|\nabla\phi| = 1$$

This information is used to initiate the level set function and then it is advected using the following form, which is same as discussed above.

$$\frac{\partial\phi}{\partial t} + (\vec{V}\cdot\nabla)\phi = 0 \tag{3.17}$$

Solving the above equation for subsequent time steps is easy and can be achieved by using appropriate advection schemes. But ψ is a distance function which is not related to the fluid properties and hence Eq.(3.16) will not be satisfied after advection and errors keep on piling after each subsequent step. Hence the level set function needs to be re-initialized as follows:

$$\frac{\partial \phi}{\partial t} = \frac{\phi_0}{\sqrt{\phi_0^2 + h^2}}(1 - |\nabla \phi|) \tag{3.18}$$

where t is the artificial time ψ_0 is the value of LS function from previous time step and h is the grid spacing. But in doing so, the mass conservation no longer holds good for the interface cells unlike the VOF scheme. Hence the LS function has to be re-distanced in every time step to satisfy the mass conservation [15] describes a re-distancing algorithm.

3.3 Coupled Level Set Volume of Fluid (CLSVOF) method and Interface Reconstruction

It is seen from earlier discussions that there exist certain limitations about using Volume of Fluid method or the Level Set method. The VOF data accurately locates the free surface and consistent with mass conservation but fails to identify the orientation fo the free surface. On the other hand, LS function gives the orientation of the free surface from the gradient of ψ but advection of this function disturbs the mass conservation law. These facts lead the discussion towards using the advantages provided by both methods and reconstruction of the free surface based on the combined information. This is the idea behind the Coupled Level Set and Volume of Fluid (CLSVOF) method [6, 16].

But there are concerns with respect to VOF and LS methods that needs to addressed. The calculation of VOF data for each cell requires information about

fluxes at cell faces which in turn needs the value of F at the cell faces. The Level Set function needs to be re-distanced to make it compatible with the mass conservation. Hence there is a need of a scheme that approximates a free surface or an interface based on the values obtained from VOF and LS data.

A Piecewise Linear Interface Construction (PLIC) scheme [17] approximates the free surface to be a straight line across the cell faces such that the volume of fluid remains consistent with the VOF data and is oriented in a direction which is consistent with the gradient of LS function. The direction is identified from the LS function as:

$$\vec{n} = \frac{\nabla\phi}{|\nabla\phi|} = \nabla\phi, \alpha = \arctan\left(\frac{n_y}{n_x}\right), (0 < \alpha < 2\pi) \tag{3.19}$$

An example of an interface constructed in a cell using PLIC scheme is shown Figure(3.4). Figure(3.5) shows a flow chart demonstrating the steps involved in CLSVOF method.

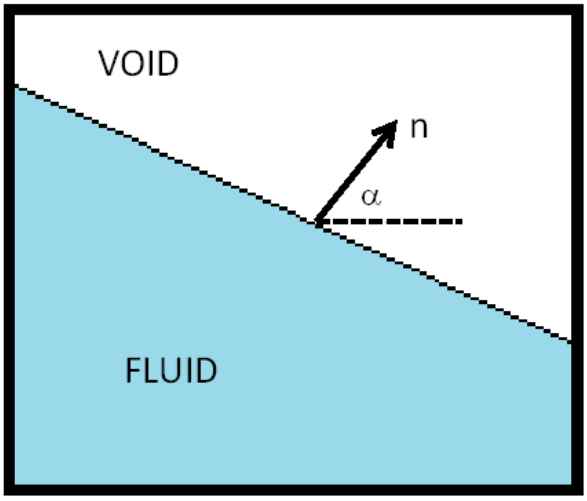

Figure 3.4: Example of interface orientation obtained from PLIC scheme.

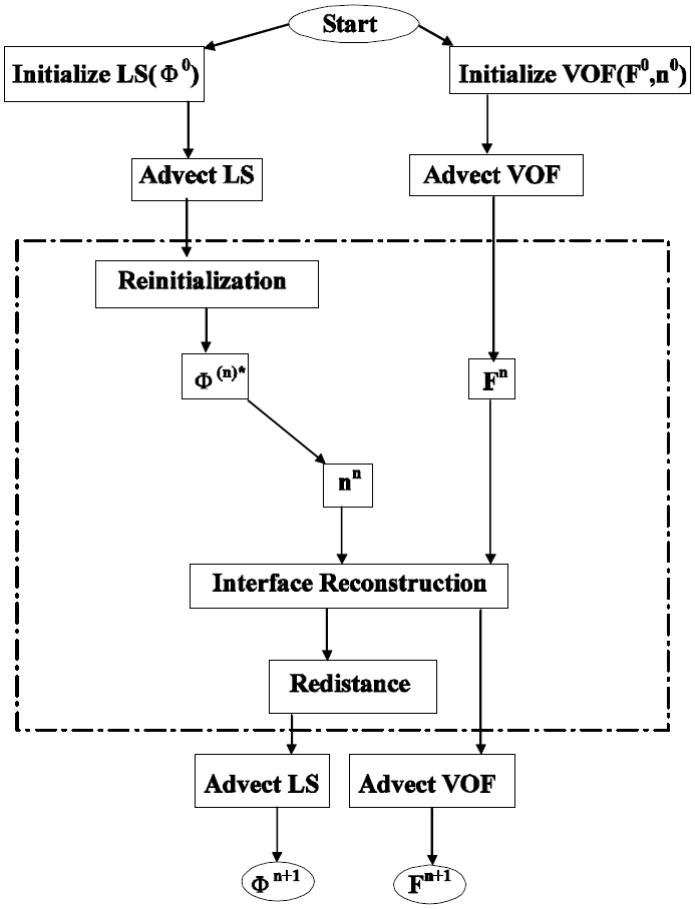

Figure 3.5: Flow chart of CLSVOF algorithm [1]

3.4 Centrifugal Force Implementation

The effect of a spinning disk is brought about in the simulation but introducing the force component in the radial direction. The computations carried out are in the cylindrical co-ordinates which solves equations in R and z directions. The two step projection scheme discussed earlier makes use of an intermediate velocity $\vec{V}$. The code has a dedicated subroutine to solve for $\vec{V}$ in order to calculate final velocities in the respective directions. The code has a provision for introducing acceleration component in horizontal direction. The term g_r in the code is made use of in order to introduce the effect of centrifugal forces in order to simulate a spinning disk. The effective force component to be introduced is given by:

$$F = m\omega^2 r \tag{3.20}$$

The parameter that is to be modeled in the vtilde subroutine is acceleration, which is $\omega^2 r$. In order to render this component effective, a time varying velocity profile formulation is used. Initializing the spin up from zero to the prescribed angular velocity is done so using exponential function and a suitable growth constant which is a function of time. The complete description of the formulation is available in [18]. The equation implemented in the code is as follows:

$$g_r = (1 - exp(-\lambda * t)) * r * (\omega * erfc(\frac{-z}{\sqrt{\nu * t}}))^2 \tag{3.21}$$

where, z is the height of the droplet at that respective instant of time, ν is the kinematic viscosity, t is the time instant and λ is the growth rate constant.

3.5 Solidification: An enthalpy based approach

The enthalpy-based energy equation is given by:

$$\frac{\partial \rho h}{\partial t} + \nabla \cdot (\rho \vec{V} h) - \nabla \cdot (\alpha \nabla h) + S_h = 0 \tag{3.22}$$

where $\alpha = k/C_p$ and S_h is a phase change source term defined as

$$S_h = \frac{\partial \rho \Delta h}{\partial t} + \nabla \cdot \rho V \Delta h \tag{3.23}$$

Rewriting Eqs.(3.20) and (3.21) in cylindrical coordinates gives

$$\frac{\partial \rho h}{\partial t} + \frac{\partial}{\partial r}(\rho u_r h) + \frac{\partial}{\partial z}(\rho u_z h) + \frac{\rho u_r h}{r} - \alpha \left(\frac{\partial^2 h}{\partial r^2} + \frac{\partial^2 h}{\partial z^2} + \frac{1}{r}\frac{\partial h}{\partial r} \right) - S_h = 0 \tag{3.24}$$

and

$$S_h = \frac{\partial \rho \Delta H}{\partial t} + \frac{\partial}{\partial r}(\rho u_r \Delta H) + \frac{\partial}{\partial z}(\rho u_z \Delta H) + \frac{\rho u_r \Delta H}{r} \tag{3.25}$$

In order to retain the dual-coordinate (Cartesian and Cylindrical) property used in the source code. Eqs (3.22) and (3.23) are reformulated into the following form.

$$\frac{\partial \rho h}{\partial t} + \frac{\partial}{\partial r}(\rho u_r h) + \frac{\partial}{\partial z}(\rho u_z h) - \alpha \left(\frac{\partial^2 h}{\partial r^2} + \frac{\partial^2 h}{\partial z^2} \right) + \zeta \left(\frac{\rho u_r h}{r} - \frac{\alpha}{r}\frac{\partial h}{\partial r} \right) - S_h = 0 \tag{3.26}$$

where S_h is given by

$$S_h = \frac{\partial \rho \Delta H}{\partial t} + \frac{\partial}{\partial r}(\rho u_r \Delta H) + \frac{\partial}{\partial z}(\rho u_z \Delta H) + \zeta \left(\frac{\rho u_r \Delta H}{r} \right) \tag{3.27}$$

where ζ takes on the values of 0 and 1 for Cartesian and Cylindrical coordinates, respectively. By defining the total enthalpy flux as $\rho V h - \alpha \nabla h$, Eq.(3.20) becomes

$$\frac{\partial \rho h}{\partial t} + \frac{1}{r}\frac{\partial J_r}{\partial r} + \frac{\partial J_z}{\partial z} = S_h \tag{3.28}$$

where

$$J_r = r \left(\rho u_r h - \alpha \frac{\partial h}{\partial r} \right) \tag{3.29}$$

$$J_z = \rho u_z h - \alpha \frac{\partial h}{\partial z} \tag{3.30}$$

and the continuity equation becomes

$$\frac{\partial \rho}{\partial t} + \frac{1}{r}\frac{\partial r \rho u_r}{\partial r} + \frac{\partial r \rho u_z}{\partial z} = 0 \tag{3.31}$$

To conform to the RIPPLE code, staggered grid is used. All variables except velocities are calculated at the intersection of the grid lines. The velocities are offset to coincide with the CV faces. The u_r velocity component is moved a half grid space to the right, and the u_z velocity component is moved a half grid up.

To account for the phase change, the governing equations have to be modified to account for the presence of both solid and liquid. The continuity equation and momentum equation become

$$\nabla \cdot (\Theta V) = 0 \tag{3.32}$$

and

$$\Theta \frac{\partial V}{\partial t} + \nabla \cdot (\Theta V V) = -\frac{\Theta}{\rho}\nabla p + \frac{\Theta}{\rho}\nabla \cdot \tau + \Theta g + \Theta F_b + S \tag{3.33}$$

respectively, where Θ is defined as the volume fraction of fluid inside a computational cell. A unit value of Θ corresponds to a cell full of fluid, whereas a zero value of Θ indicates that the cell contains all solid or obstacle. When Θ takes a value between 0 and 1, the corresponding cell has both fluid and solid. The VOF transport equation is changed to

$$\frac{\partial}{\partial t}(\Theta F) + \nabla \cdot (\Theta F V) = 0 \tag{3.34}$$

Note that these equations reduce to Eqs(3.1) and (3.2) when Θ takes a value of 1. The source term takes the following form $S = -Au$, where $A = -C(1-\Theta^2)/(\Theta^3 + \epsilon)$, which is used to modify the momentum equation in the

dendritic mushy region, where the fluid is modeled flowing through the porous media. The value of C will depend on the morphology of the porous media, and ϵ is a small number used to avoid division by zero. When the computational cell is in liquid phase the Θ has a value of 1, the source term has no effect. However as the cell changes its phase the source term grows and dominates over the transient, convective and diffusive components of the momentum equation. This source term models the flow in a porous media defined by the Carman-Kozeny equation given by

$$\frac{\nabla P}{\rho} = -\left(C\frac{(1-\Theta)^2}{\Theta^3}\right)V \tag{3.35}$$

When the computational cell reaches the solid phase, the source term is so large that it dominates all components of the momentum equation and forces the velocities to zero (implying solidification). The complete details of the solidification formulation adopted in this code can be found in [19].

The free surface construction is done using PLIC scheme representing the interface as a straight line within a computational cell. The momentum and thermal flux calculations across cell faces containing interfaces need special accounting. Such cell faces are partial and the governing equations are not integrated throughout the complete face. The wetting ratios are defined for each cell.
Integrating Eq(3.27) over the control volume gives:

$$\frac{(\rho_p h_p - \rho_p^o h_p^o)\Delta r \Delta z}{\delta t} + \frac{1}{r}(J_e - J_w) + (J_n - J_s) + S_h \Delta r \Delta z = 0 \tag{3.36}$$

The continuity equation integrated over the control volume gives:

$$\frac{(\rho_p - \rho_p^o)\Delta r \Delta z}{\delta t} + \frac{1}{r}[(\rho u)_e - (\rho u)_w] + [(\rho v)_n - (\rho v)_s] = 0 \tag{3.37}$$

Multiplying Eq(3.37) with h_p and subtracting from Eq(3.36) gives:

$$\begin{aligned}\frac{(\rho_p h_p - \rho_p^o h_p^o)\Delta r \Delta z}{\delta t} + \frac{\Delta z}{r_p}[(J_e - r_e(\rho u_r)_e h_e) - (J_w - r_w(\rho u_r)_w h_w)] + \\ \Delta r[(J_n - r_n(\rho u_z)_n h_n) - (J_s - r_s(\rho u_z)_s h_s)] + S_h \Delta r \Delta z = 0\end{aligned} \tag{3.38}$$

The above equation can be modified as

$$\begin{aligned}\frac{\rho_p(h_p - h_p^o)\Delta r \Delta z}{\delta t} + \frac{\Delta z}{r_p}[aw_e(J_e - r_e(\rho u_r)_e)h_e - aw_w(J_w - r_w(\rho u_r)_w)h_w] \\ + \Delta r[aw_n(J_n - r_n(\rho u_z)_n)h_n - aw_s(J_s - r_s(\rho u_z)_s)h_s] + S_h \Delta r \Delta z = 0\end{aligned} \tag{3.39}$$

with the source term being

$$b = a_p^o(\delta h_p - \delta h_p^o) + (inflow - outflow) + a_p^o \delta h_p^o (F_p - F_p^o) \tag{3.40}$$

where the last term represents the enthalpy correction due to mass inflow or outflow over a particular time step. Eq(3.39) suggests that multiplying the F and D terms is sufficient to account for the partial face fluxes near the surface.

CHAPTER 4

Problem setup, Results and Discussion

Numerical study of fluid flow in spin coating process is assumed to be incompressible. As mentioned earlier, the code uses a finite volume method on a fixed uniform grid in cylindrical coordinate system. A grid sensitivity test has to be performed to decide the grid size that accurately models the flow. The free surface (interface) is obtained using the CLSVOF method with a PLIC scheme. The numerical and fluid parameters used in the study are included in the input file listed in the Appendix (A).

4.1 Geometrical Setup

The first step involved in the problem setup is to create a geometry that projects the desired kind of flow without the loss of any information. The problem setup in case of spin coating process is to model the droplet on the substrate.
The following assumptions are made in the analysis:

- the plane is horizontal, so that there is no radial gravitational component
- the liquid layer is radially symmetric, and so thin that differences in gravitational potential normal to the surface of the disk have negligible effect in distributing the liquid compared with the effect of centrifugal forces,
- the viscosity is independent of the rate of shear, i.e., the liquid is Newtonian,
- the liquid layer is everywhere so thin that shear resistance is appreciable only in horizontal planes,

- the radial velocity is everywhere so small that Coriolis forces may be neglected,
- the evaporation of the fluid is negligible

The substrate in the analysis is a isothermal surface, wherein the temperature of the surface is assumed to be held rigidly at a temperature. The temperature of plate is modified using the input section of the code. This information is fed to the code with input variables that control related functions in the problem setup. There are seven major sections. They are (1)NUMPARAM for numerical parameters; (2)FLDPARAM, for fluid parameters; (3)MESH, for mesh generation; (4)OBSTCL, for setting interior obstacles; (5)FREESURF, for initializing the free surfaces; (6)GRAPHICS, for generating dynamic graphics.(7) HEATEQ, for heat transfer mechanisms.

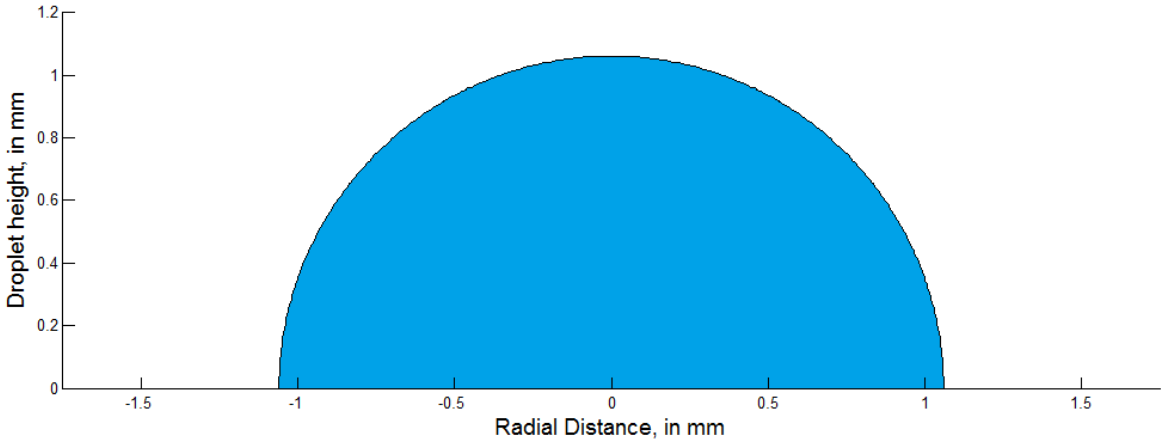

Figure 4.1: Initial problem setup: Droplet and Substrate

In Figure(4.1), the x-axis is the substrate. The heat transfer is in the downward direction and the solidification occurs from bottom in the upward direction

as the region of the droplet coming in contact with the substrate solidifies first and it progresses with time.

4.2 Boundary Conditions

Boundary conditions play vital role in controlling the simulation of the flow. The inner edges of the domain of interest are associated with boundary conditions as mentioned below:

Boundary Region	Boundary Condition
Left Boundary	Rigid Free Slip
Right Boundary	Continuative Outflow
Bottom Boundary	Rigid No-slip
Top Boundary	Rigid Free Slip

Rigid No-slip or wall boundary condition implies that the velocity at that particular face is zero and there is no flow across that face. Continuous outflow means that the gradient of velocity in a direction perpendicular to that face is zero. Rigid free slip boundary condition allows the fluid to move freely over the surface without offering any resistance.

4.3 Grid Refinement study:

A grid refinement study was carried out in order to select a computational domain of suitable resolution. Figure(4.2) shown below is a compound plot of all the grid resolutions used. A uniform square grid is used. A series of cases were run with changing grid resolution from a coarse one with $0.04mm$ to $0.005mm$ with successive reduction in grid size by 50%. Grid dimensions of $0.04mm$ and $0.02mm$ failed to converge especially at higher angular velocities. The relative error was found to be vary between 0.2% and 0.6% for successive grid size reduction from

$0.01mm$ to $0.005mm$. Hence, grid size of $0.01mm$ was selected for the studies which was carried out further. Suitable changes were made in various parts of the code in order to bring the effects of spreading under the action of centrifugal force and solidification occurring due to heat transfer between substrate and droplet. The contour in blue represents a case with grid resolution of $0.02mm$, the one plotted in black color corresponds to grid resolution of $0.01mm$ and red represents a grid resolution of $0.005mm$.

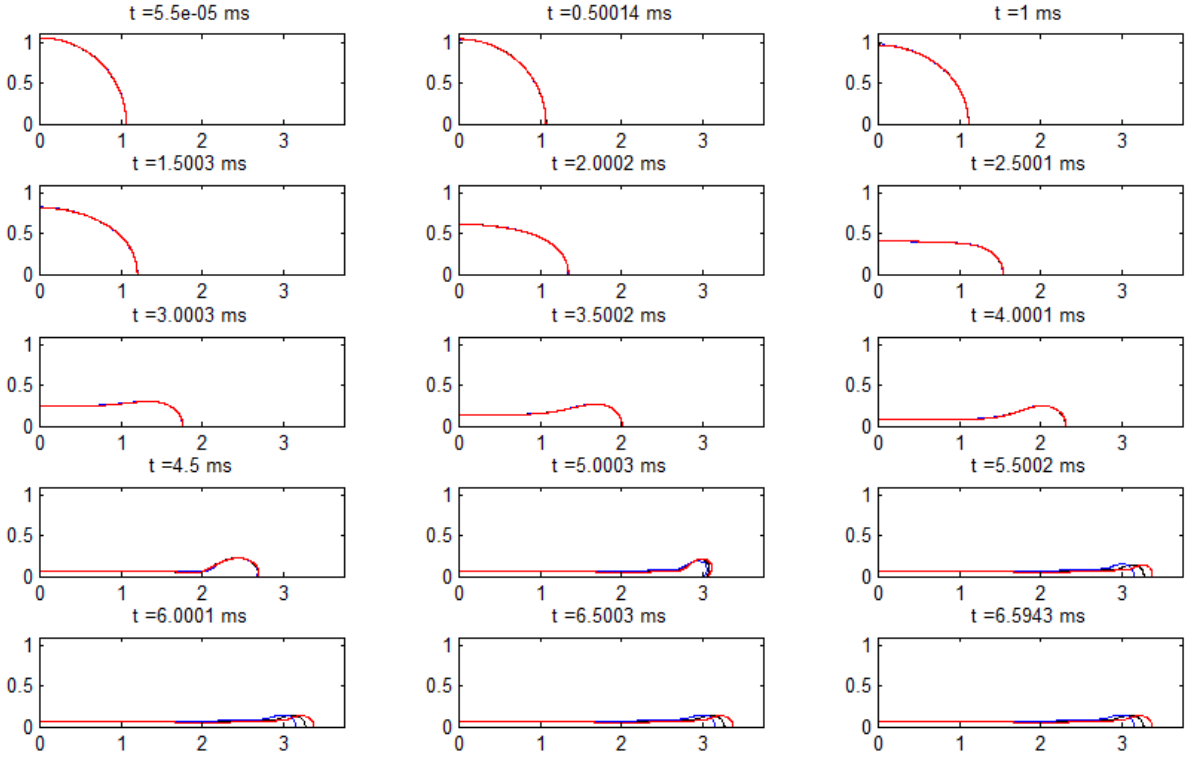

Figure 4.2: Grid refinement study

4.4 Reference Case

The standard case taken is the droplet which is rotated at $3000RPM$. The specifications of the standard case is as mentioned in the table below:

Parameters	Value(SI units)
Grid Dimensions(X x Y)	400x120
Cell Spacing	$0.00001m$
Droplet Diameter	$0.0010607m$
Droplet Density	$6950kg/m^3$
Surface tension	$0.55N/m$
Kinematic Viscosity	$1.8 * 10^{-7}m^2/s$
Initial droplet temperature	$1100K$
Substrate temperature	$500K$
Specific heat capacity	$240J/kg - K$
Droplet thermal conductivity	$66.8W/m - K$
Substrate thermal conductivity	$66.8W/m - K$
Latent heat of phase change	$59kJ/kg$
Melting point of Tin	$505.08K$

.

In Figure(4.3), the contour marked in red represents the solidification front. The droplet begins to spread due to the centrifugal force. In addition to spreading under the influence of force, it begins to solidify. The solidification front progresses in the upward direction as the droplet is held $600K$ above the substrate temperature. We come to the conclusion that the whole droplet has solidified when the red contour has merged with the free surface, this implies that the temperature of the droplet is below the melting point of the metal used in the study. In the reference case, the entire process of spreading and solidification occurs over a time

period of $8.26ms$. Due to force acting in the radial direction, droplet experiences a force equal to $m\omega^2 r$. Due to force being a function of distance from the axis of symmetry, bulk of the fluid moves towards the leading edge forming a bead like structure. Solidification first occurs in the region close to axis as the layer of fluid is thin. The region where the solidification occurs towards the last is at the leading edge.

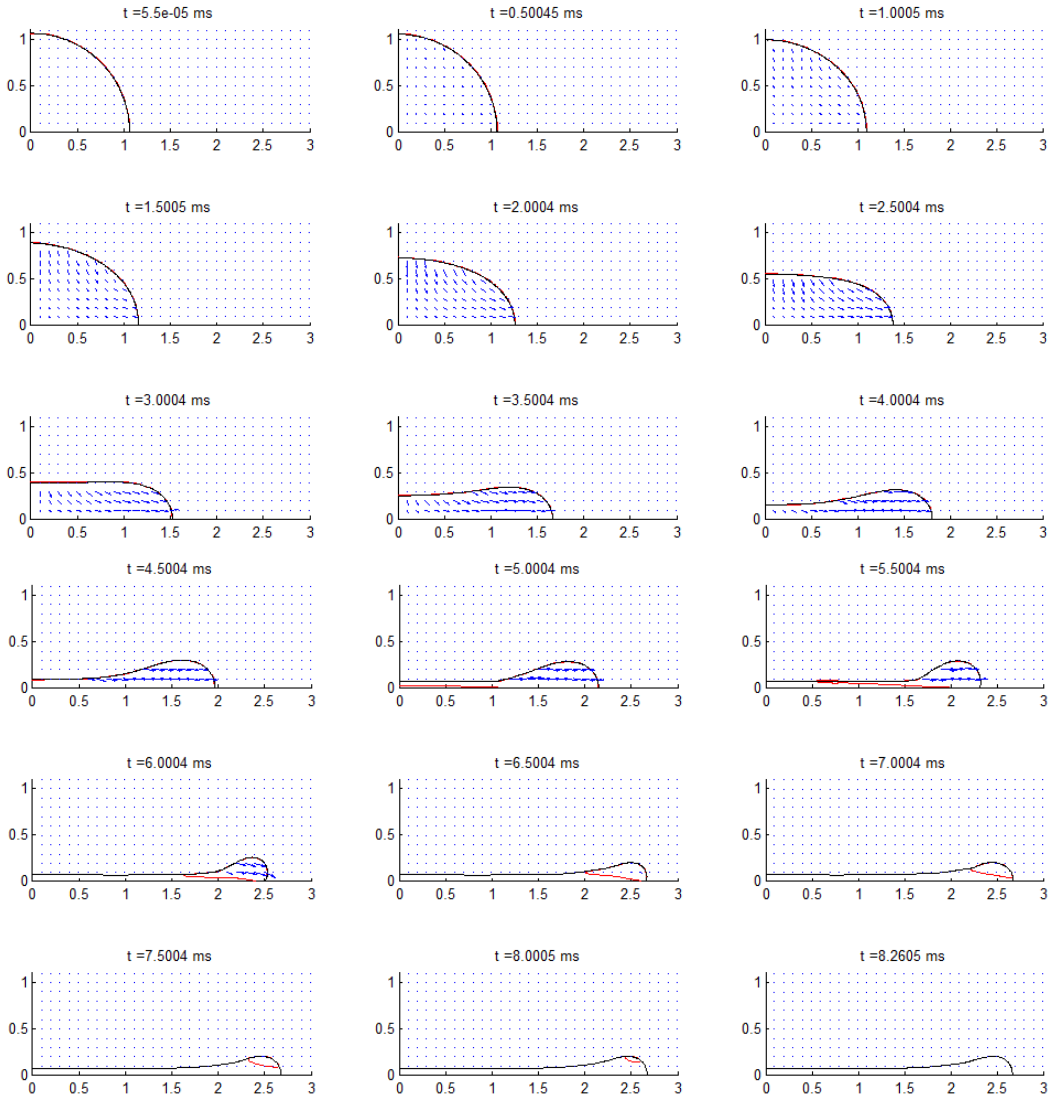

Figure 4.3: Reference case

4.5 Flow Profile Evolution

The Figure(4.4) shown below consists of a series of images overlapped, each of the images is taken at successive time instants. A similar profile has been obtained by [2] as shown in Figure(4.5).

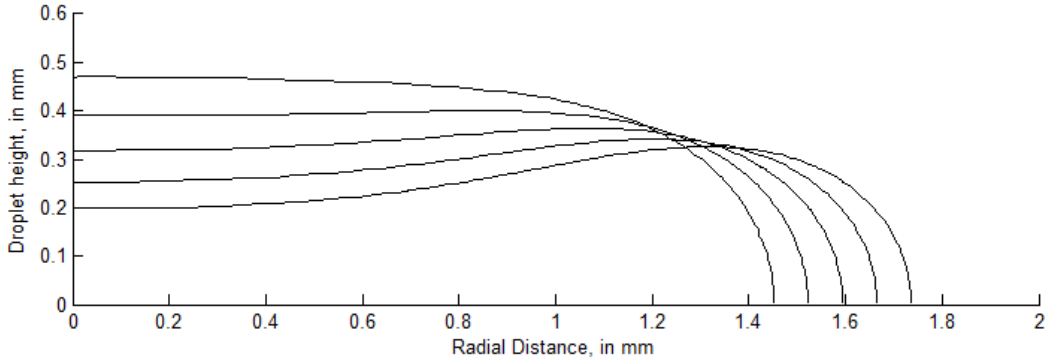

Figure 4.4: The free surface profile obtained from the current study

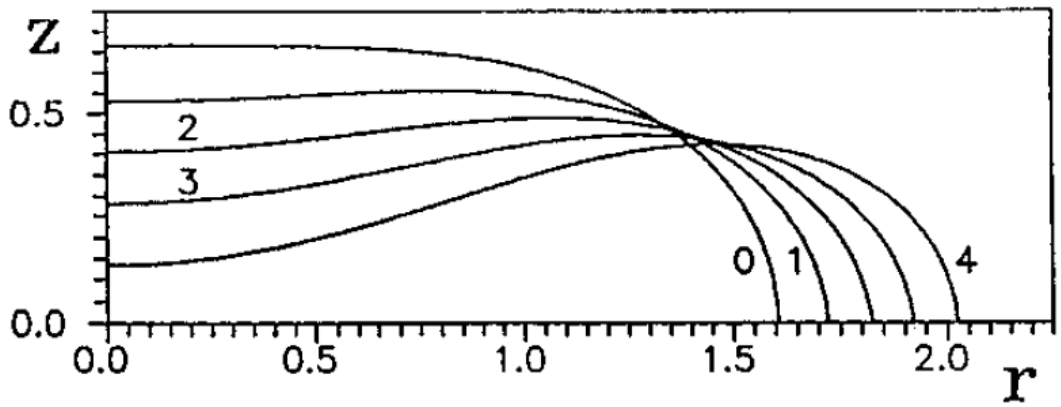

Figure 4.5: The free surface profile obtained from [2]

Force experienced by the fluid increases as the fluid progresses in the radial direction, this causes the fluid to bulge towards the leading edge of the droplet. The droplet experiences relatively low magnitude force in regions closer to sym-

metric axis. The accumulation of fluid towards the leading edge of the droplet is referred to as edge bead effect. This bead formation in the leading edge region of the droplet under the action of the centrifugal force is undesirable as this causes uneven surface. There are special methods employed to remove these edge beads. One such method is to discharge more than adequate volume of the fluid and allow the material to spin off from the substrate there by avoiding the formation of edge bead.

4.6 Parametric Studies

A parametric study is a series of simulations where one or more parameters of the problem are varied to investigate the sensitivity of the solution to the parameters. Parametric studies are an important aspect of CFD analysis. Parametric studies are used to perform trend base analyses. The parameters that are of importance in this study are:

- Effect of Angular Velocity on thickness and extent of spread.
- Effect of Spin up rate on the extent of spread and final thickness obtained.
- Effect of Substrate Temperature.
- Effect of Initial Droplet Temperature.
- Effect of Latent Heat.

4.6.1 Effect of Angular Velocity on thickness and extent of spread

The key parameter in the present study is the spin speed/angular velocity of the substrate. It is an indicator of magnitude of centrifugal force acting on the droplet. Several cases were carried out with varying spin speed. The variation of which was between $1000RPM$ to $4000RPM$ in steps of $500RPM$. It was found that for spin speeds up to $2000RPM$ the spreading was limited due to surface tension of the droplet resisting the centrifugal force trying to drive the fluid radially outwards. For spin speeds greater than $2500RPM$, the spreading was evident as surface tension was overcome by centrifugal force. The effect of angular velocity on the thickness of coating and extent of spread achieved is as shown in the Figure(4.6) below. It is seen that thickness of coating decreases with increasing angular velocity and extent of spreading increases with increase in angular velocity. This is because higher spin speed implies larger centrifugal force.

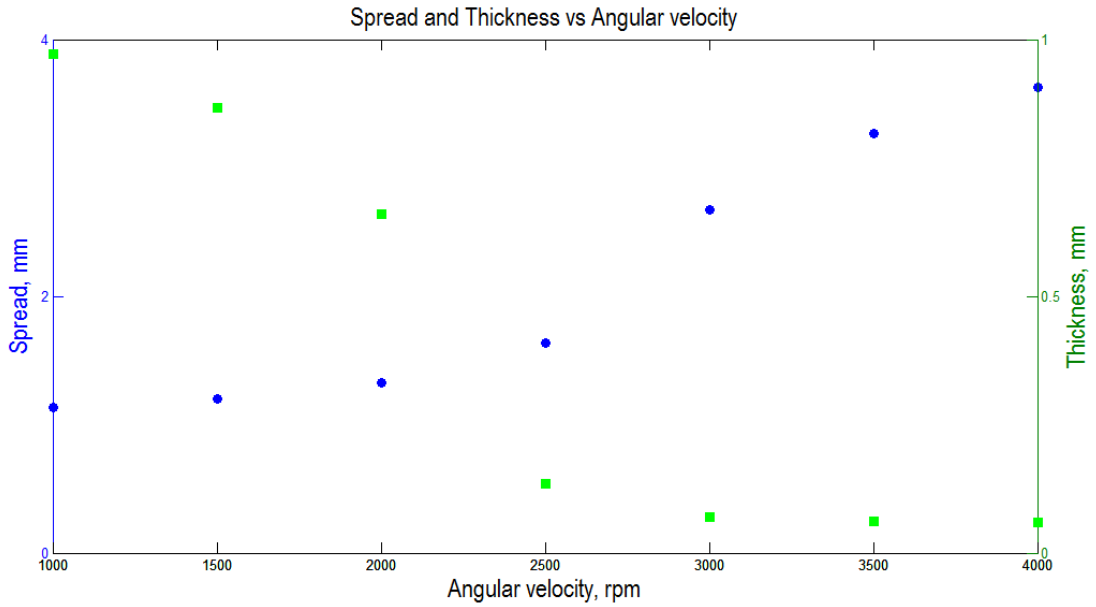

Figure 4.6: Spin speed vs thickness and spread

The Figure(4.7) below depicts free surface contours after the solidification is complete. It is seen that free surface corresponding to $1000RPM$ has hardly spread, reason for this being surface tension of the droplet is much higher that the magnitude of centrifugal force applied. In general, the thickness of a spin coated film is proportional to the inverse of the spin speed squared as in the below equation where t is the thickness and ω is the angular velocity:

$$t \propto \frac{1}{\sqrt{\omega}} \tag{4.1}$$

Change in angular velocity affects the solidification rate. Lower spin speed implies lesser spreading implying more mass of fluid over a given area of the substrate. This leads to more heat to be drained at the droplet-substrate interface causing the droplet to solidify at a slower rate. Whereas solidification in case of higher angular velocity is lot quicker as the droplet spreads more giving more area for film and substrate contact. This results in rapid flow of heat into the substrate thereby leading to reduced solidification time.

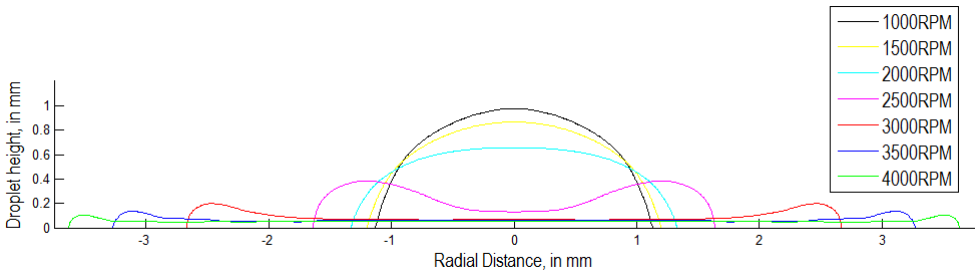

Figure 4.7: Final free surface contours after the completion of solidification

The exact thickness of a film will depend upon viscosity, temperature. Typically a test film is spin coated and the thickness measured either by ellipsometry or surface profilometry. From this one or more data point(s) the spin thickness

curve can be calculated usually with a good degree of accuracy. The spin speed can then be adjusted to give the desired film thickness. This dependence upon the square root of spin speed is both an advantage and a disadvantage. The disadvantage is that it means that the range of thicknesses that can be achieved from a given solution spans a relatively narrow range. On the other hand the advantage is that it allows precise control of film thickness within this range.

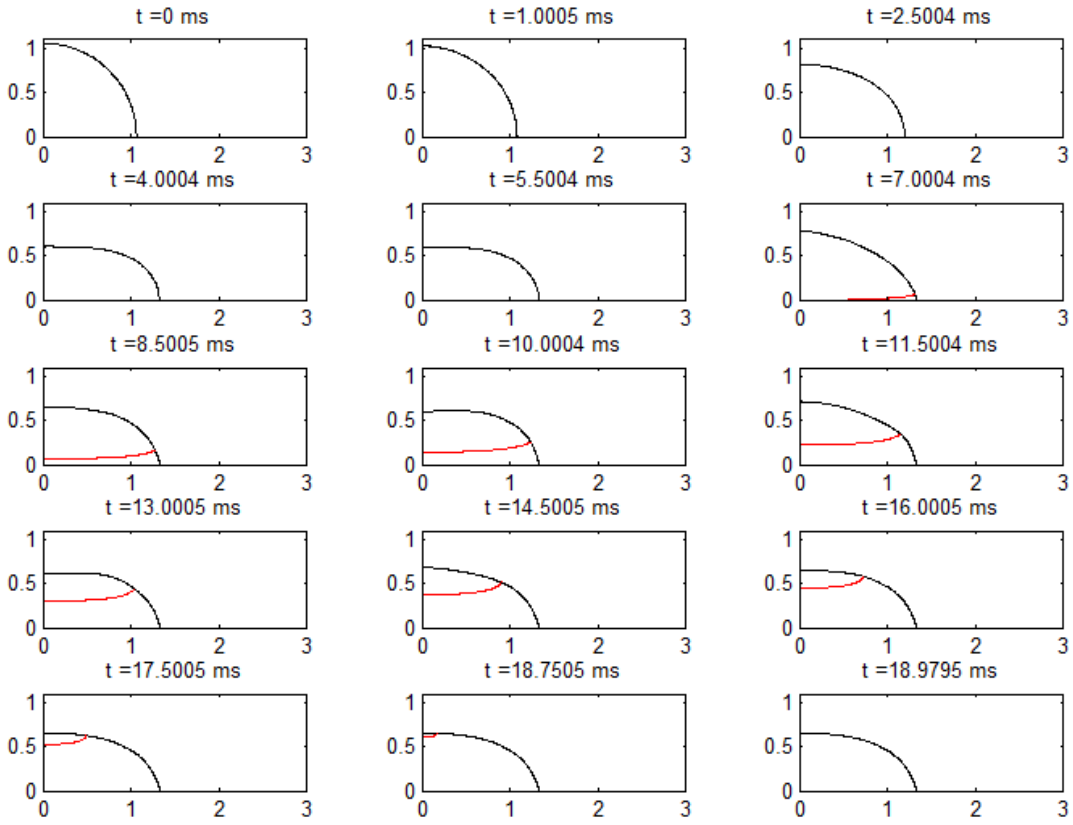

Figure 4.8: Spreading of droplet corresponding to an angular velocity of 2000 RPM

The Figure(4.8) above shows the time lapse frame for an angular velocity of $2000RPM$. Due to surface tension being the dominating force, it is seen that droplet doesn't spread effectively. Solidification time for this case is found to be

18.97ms. This is because lower spin speeds result in thicker splats and the amount of heat that needs to be rejected to the substrate occurs over a smaller area.

The Figure(4.9) shown below, is the case with angular velocity of 4000RPM. It is observed that due to higher spin speed, the centrifugal force is the dominant force in comparison to surface tension of the droplet, which results in spreading to greater extent. The extent of spread and thickness for this case is found to be 3.63mm and 60μm respectively. The solidification time is 5.5465ms. This is because greater extent of spread has paved way for more area for the heat transfer to occur. In addition to the larger area, the fluid layer on the substrate is thin aiding the process of solidification.

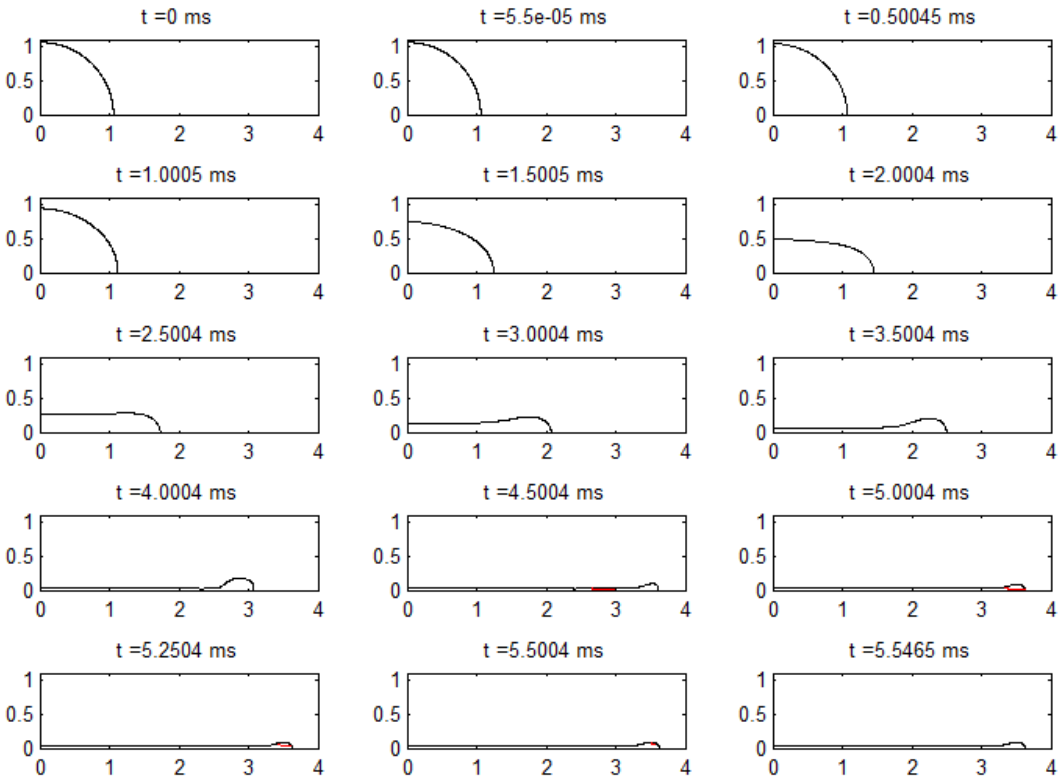

Figure 4.9: Spreading of droplet corresponding to an angular velocity of 4000 RPM

4.6.2 Effect of Spin up/ Ramp rate on final thickness obtained

Spin up is a phase where the substrate is accelerated up to its final, desired angular velocity. This is a stage which usually is characterized by aggressive fluid movement in the radial direction. Spiral vortices may be present during this stage. These would form as a result of the twisting motion caused by the inertia that the top of the fluid layer exerts while the substrate below accelerates. Eventually, the fluid is thin enough and can be considered stationery with respect to the rotating substrate resulting in fluid thickness differences to disappear soon after the substrate reaches the final desired angular velocity. Accelerating the substrate to final spin speed is done using exponential function. Much of work published on the spin coating addresses the effect of spin speed on the final thickness achieved. In the present study an attempt has been made to study the effect of ramp rates. The Figure(4.10), below shows the variation of thickness and spread for varying ramp rates.

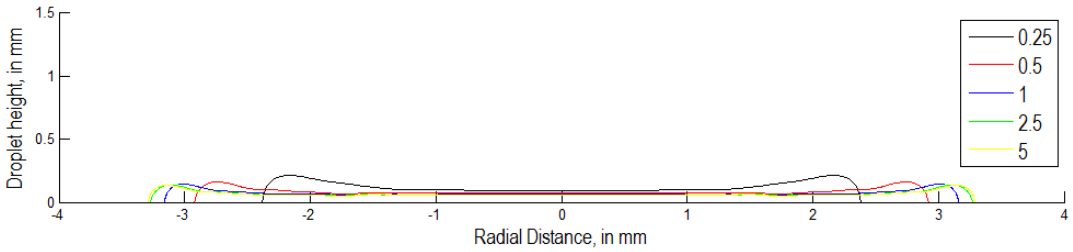

Figure 4.10: The extent of spread and thickness variation due to change in ramp rate.

Effect of ramp rate was studied with an angular velocity of $3500RPM$. The ramp rates for which the cases were carried out were $1 - \exp(\lambda t)$, where λ took the values: $0.25, 0.5, 1, 2.5, 5$, where a larger value of λ implies higher ramp rate.

Figure(4.11) below shows the time taken for various ramp rates to reach

100% of the angular velocity specified in the input file. It can be inferred from that for a ramp rate corresponding to $\lambda = 5$ the spreading is the largest and for $\lambda = 0.25$ the spreading is lowest.

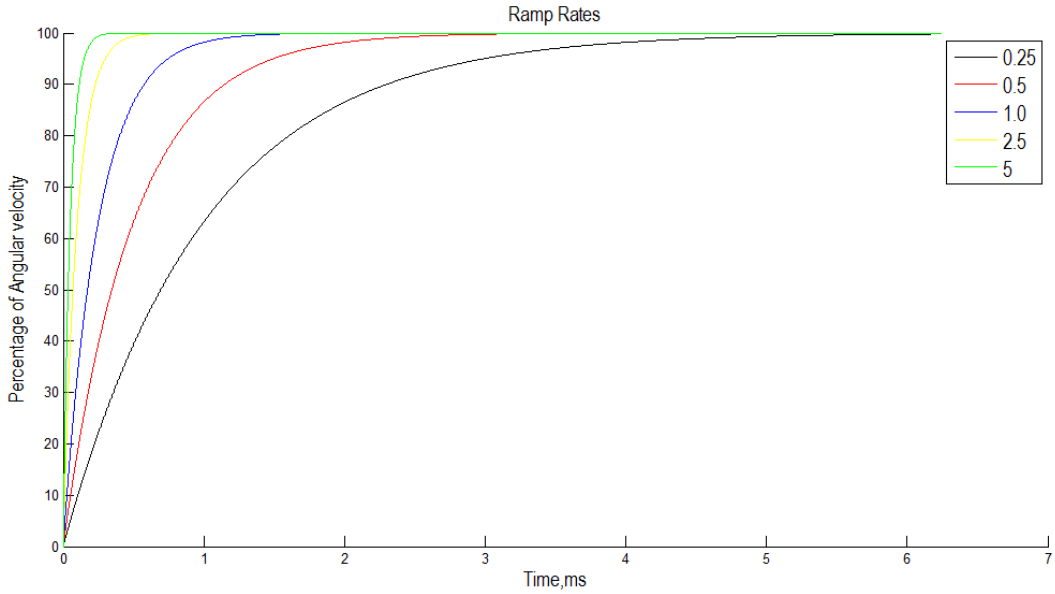

Figure 4.11: Time taken vs percentage of angular velocity achieved

Ramp rate affects the thickness of the spread. For a value of $\lambda = 5$ in the above expression, acceleration produced is maximum and it results in thickness being minimum when compared to all other ramp rates. And for a value of $\lambda = 0.25$, the thickness of the coat is maximum as acceleration produced in this case is least.

Solidification occurs rapidly in the case where $\lambda = 5$ as thickness produced in this case is least, resulting in lower heat flux into the substrate. And for $\lambda = 0.25$ thicker coat is produced leading to larger solidification time.

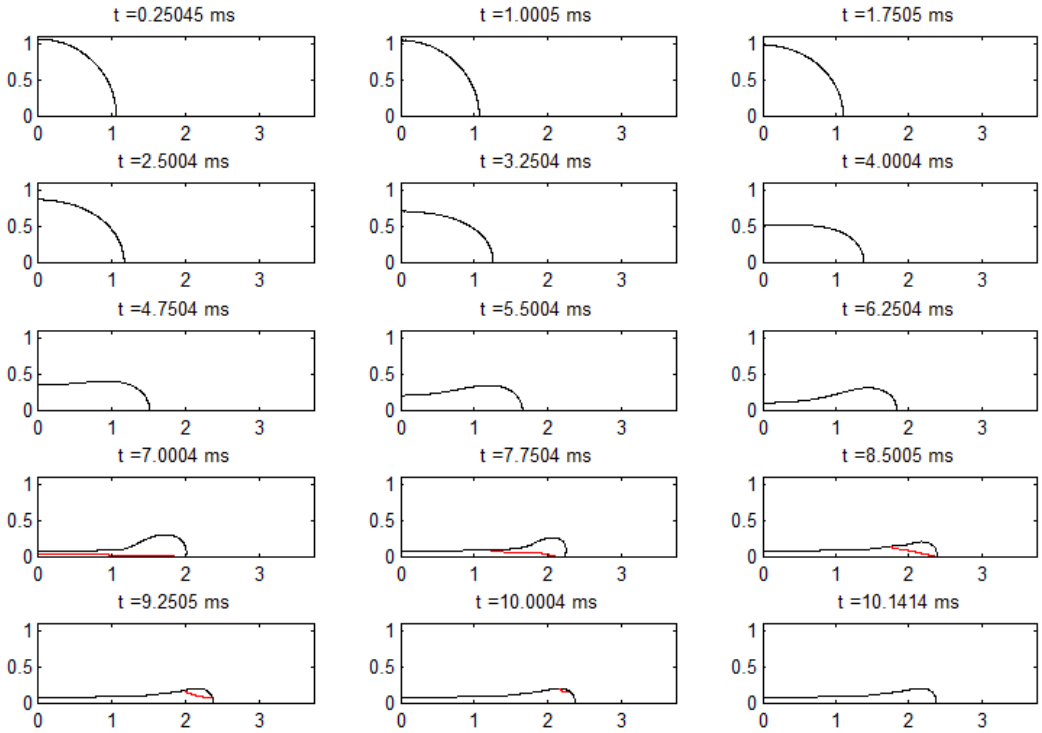

Figure 4.12: Ramp rate λ=0.25

The Figure(4.12) above shows the spreading of droplet subjected to a ramp rate constant of $\lambda = 0.25$. The solidification process is complete at $t = 10.1414ms$ with a thickness of $90.5\mu m$ and spreading over radius of $2.38mm$

Figure(4.13) shows the spreading of droplet subjected to a ramp rate constant of $\lambda = 2.5$. The solidification process is complete at $t = 6.5874ms$ with a thickness of $61.5\mu m$ and spreading over radius of $3.27mm$

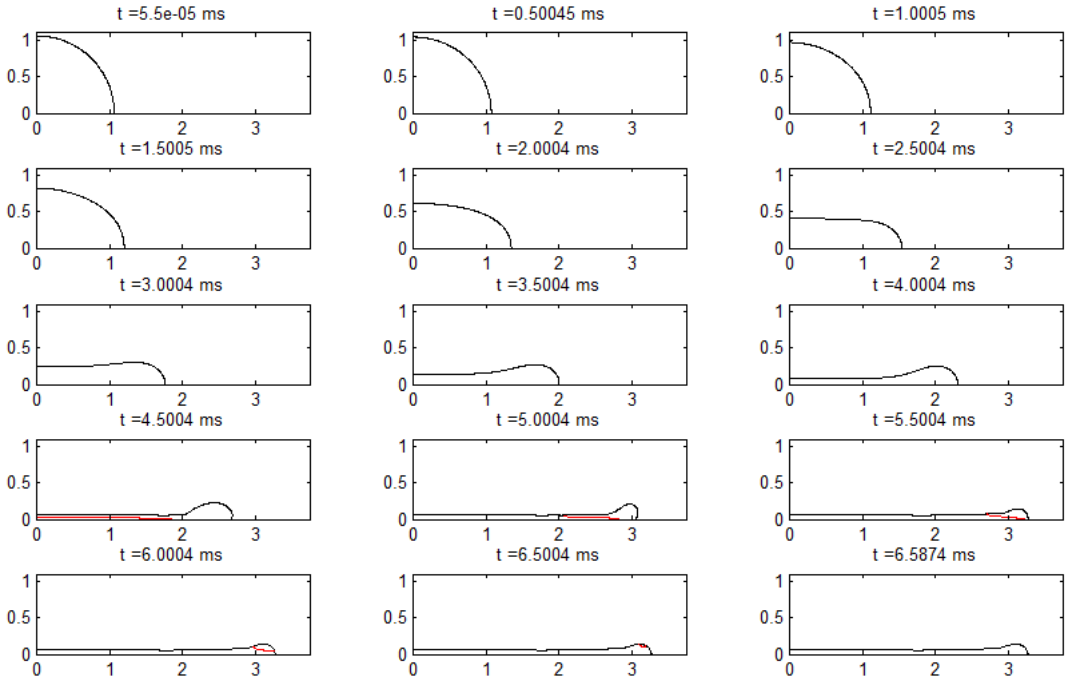

Figure 4.13: Ramp rate λ=2.5

The Figure(4.14) below shows variation of thickness for varying ramp rate constants. It is seen that for $\lambda = 0.25$, the time taken to reach specified angular velocity is approximately $6ms$. The film thickness is $300\mu m$. For $\lambda = 5.0$, time taken to reach the specified angular velocity is less than $1ms$. This difference in the time taken to reach the angular velocity specified results in thickness variation as acceleration produced in case of $\lambda = 5$ is larger than $\lambda = 0.25$. As mentioned previously present study used tin as coating material and molten tin is Newtonian fluid with solidification occurring simultaneously as the droplet spreads.

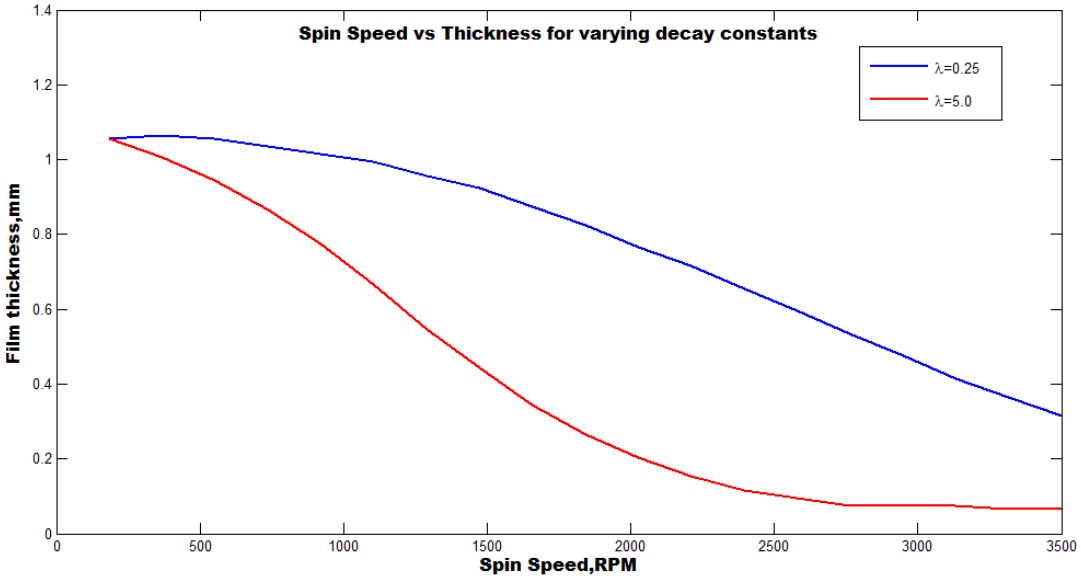

Figure 4.14: Variation of thickness as a function of ramp rate constant

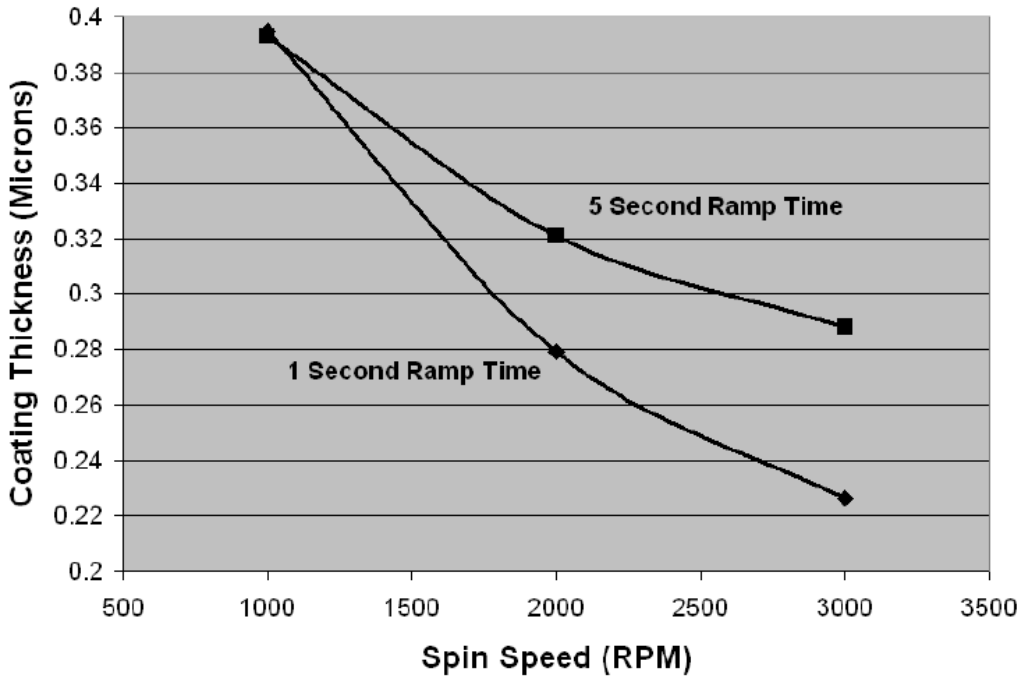

Figure 4.15: Variation of thickness as a function of ramp rate constant obtained from [34]

The Figure(4.15) above is obtained from [34] where thickness versus spin speed is plotted for different values of acceleration. The study emphasizes the effect of ramp up stage in spin coating process. The solution used is Non-Newtonian and does not involve solidification. But there is a good qualitative agreement between the two.

4.6.3 Effect of Substrate Temperature

The effect of substrate preheating on the spreading and solidification of individual molten droplet in spin coating has been investigated. If there is sufficient heat transfer between the droplet and substrate. The edges of the droplet freeze while it is still spreading. This obstructs the flow of liquid and produces an irregular splat. On the other hand, if there is low heat transfer from the droplet (as is the case when it is on a hot substrate, or if there is large thermal contact resistance between the droplet and substrate) it spreads completely before solidifying and produces a circular splat.

This study was carried out by varying the temperature of the substrate from $400K$ to $475K$ in steps of $25K$. The droplet is held at constant temperature of $1100K$. This leads to a different rate at which heat is rejected to the substrate thereby changing the time needed for solidification each case. The Figure(4.16), shown below depicts the variation of thickness and spread for varying substrate temperatures.

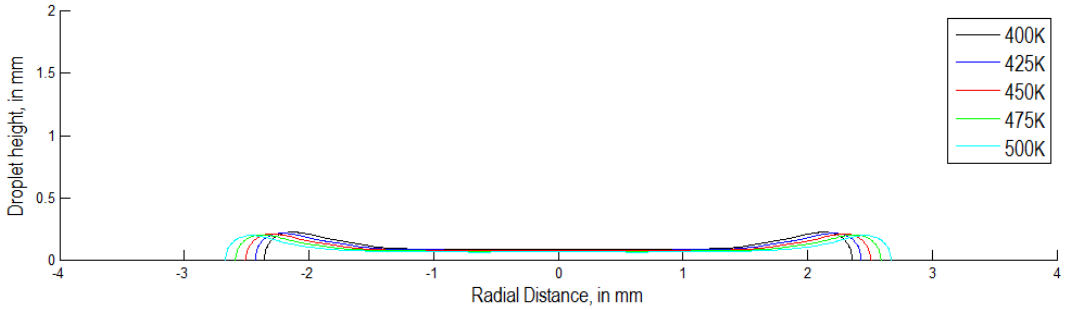

Figure 4.16: Effect of substrate temperature variation

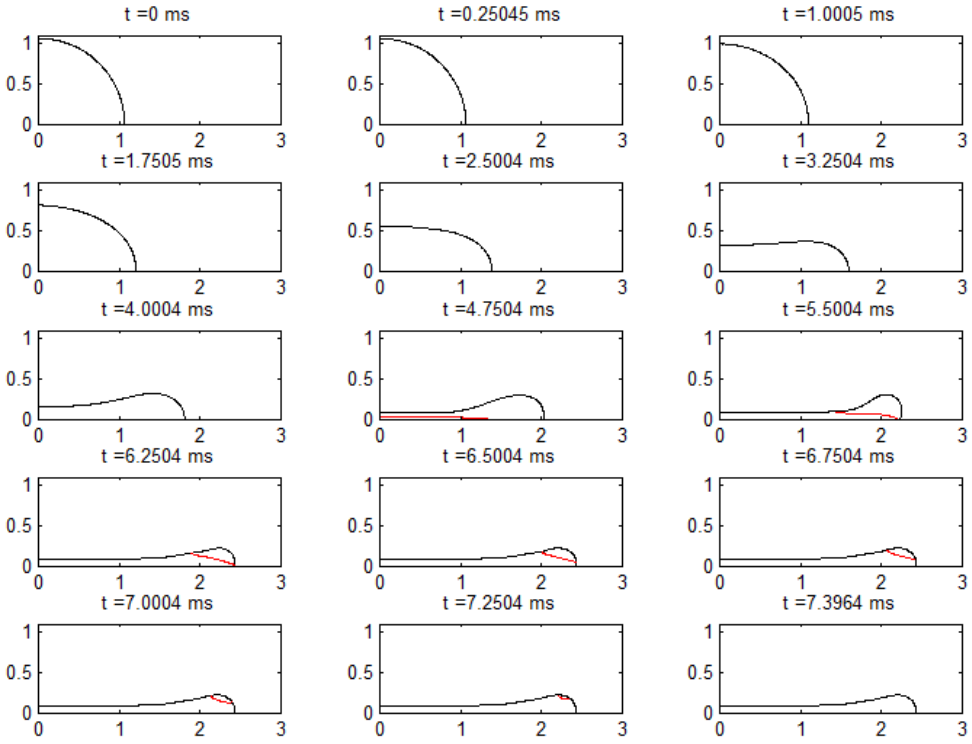

Figure 4.17: Droplet spreading with substrate temperature of 425 K

The Figure(4.17) above is the time lapse for a case with substrate temperature of $425K$. It is observed that solidification begins at $t = 4.75ms$ and the coating is completely solidified at $t = 7.396ms$. The extent of spread in this case

is 2.43mm.

The Figure(4.18) below corresponds to temperature of 475K. The solidification process begins at $t = 4.75ms$ and is complete at $t = 7.924ms$. The spreading in this case is found to be 2.59mm. It is evident from the figures that case with substrate temperature 425K solidifies prior to the case where temperature is held at 475K, and as a result of this, spreading is more for the case where substrate temperature is held at 475K.

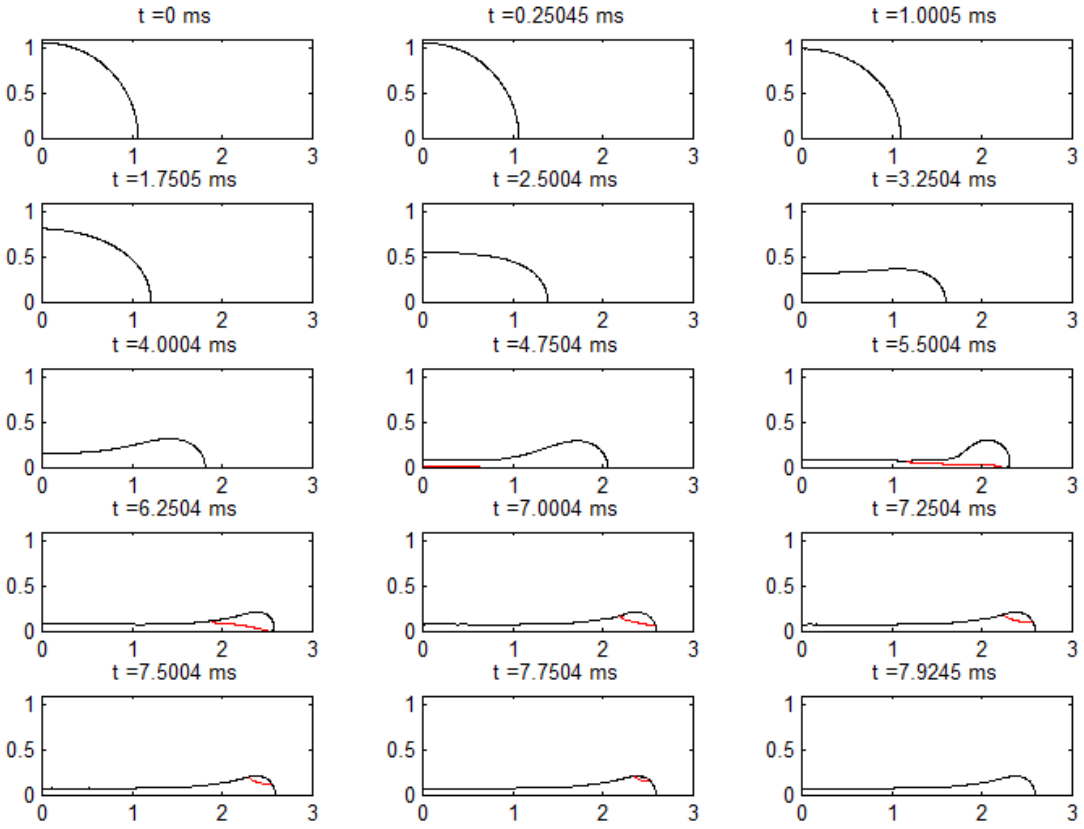

Figure 4.18: Droplet spreading with substrate temperature of 475 K

4.6.4 Effect of Initial Droplet Temperature

The process of solidification in the present study does not include substrate remelting. The substrate is held at a constant temperature. It acts as an infinite heat sink i;e irrespective of the amount of heat transferred, there is no change in the temperature of the substrate. In general, pure metals have very small or no mushy region. Difference of $1K$ is used between the solidus and liquidus temperatures.

Droplet temperature has a direct influence on the solidification. This parameter directly controls the flattening degree through the rate of solidification in addition to the angular velocity having its influence on of spreading and flattening rate. Change in droplet temperature changes the sensible heat.

Simulations for droplet temperature values between $800K$ and $1300K$ in steps of $100K$ are carried out, as shown in Figure(4.19). The substrate as mentioned earlier is held constant at a temperature of $500K$.

The plot below shows the variation of thickness and spread for different values of droplet temperatures. It is observed that as droplet temperature increases the spreading increases. Larger the temperature difference between the substrate and droplet, larger is the time required to solidify. The rate of solidification is the slowest in case of the droplet with temperature of $1300K$. Slower rate of solidification allows additional spreading of the droplet.

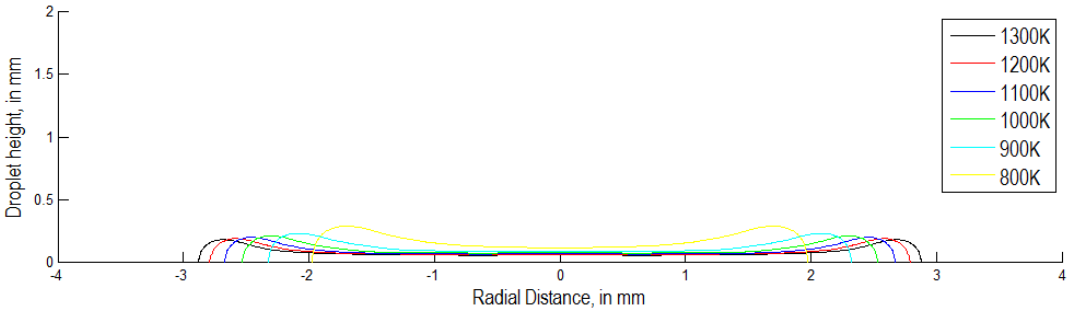

Figure 4.19: Effect of initial droplet temperature variation

Figure(4.20) shows of spreading of the droplet with an initial temperature of $900K$ at different time instants. It is observed that the solidification process is complete at $t = 8.0864ms$. The extent of spread in this case is $2.32mm$ and thickness at the center of the droplet is found to be $90\mu m$

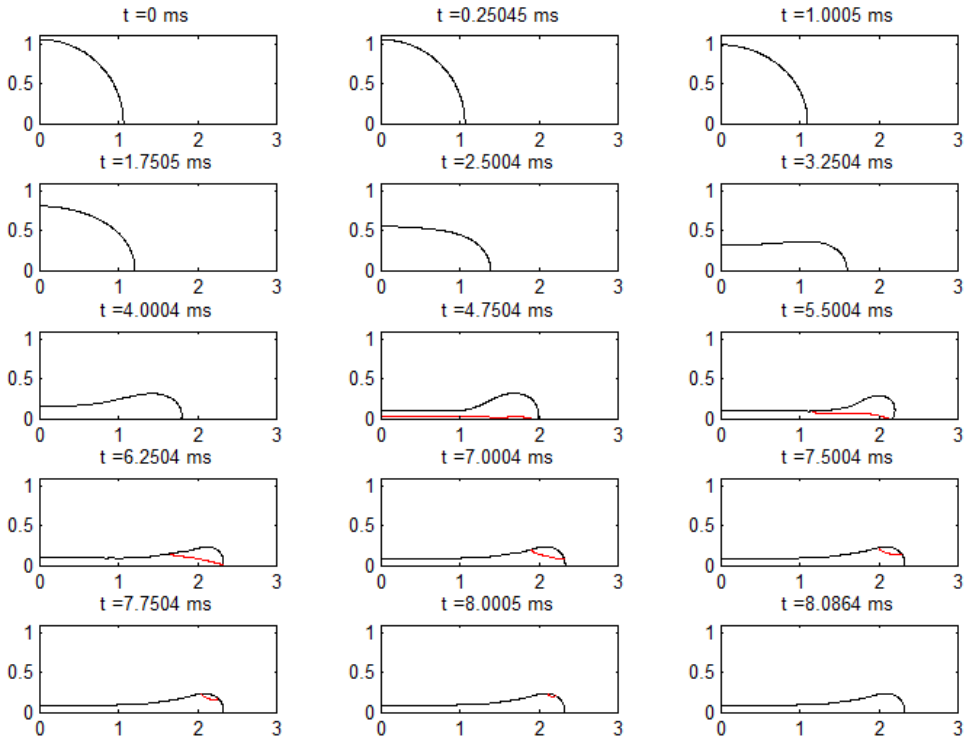

Figure 4.20: Droplet with an initial temperature of 900 K

The Figure(4.21) below shows the droplet spreading with an initial temperature of $1300K$. It is seen that solidification process is complete at $t = 8.3644ms$.The extent of spread in this case is $2.88mm$ and thickness at the center of the droplet is found to be $60\mu m$.

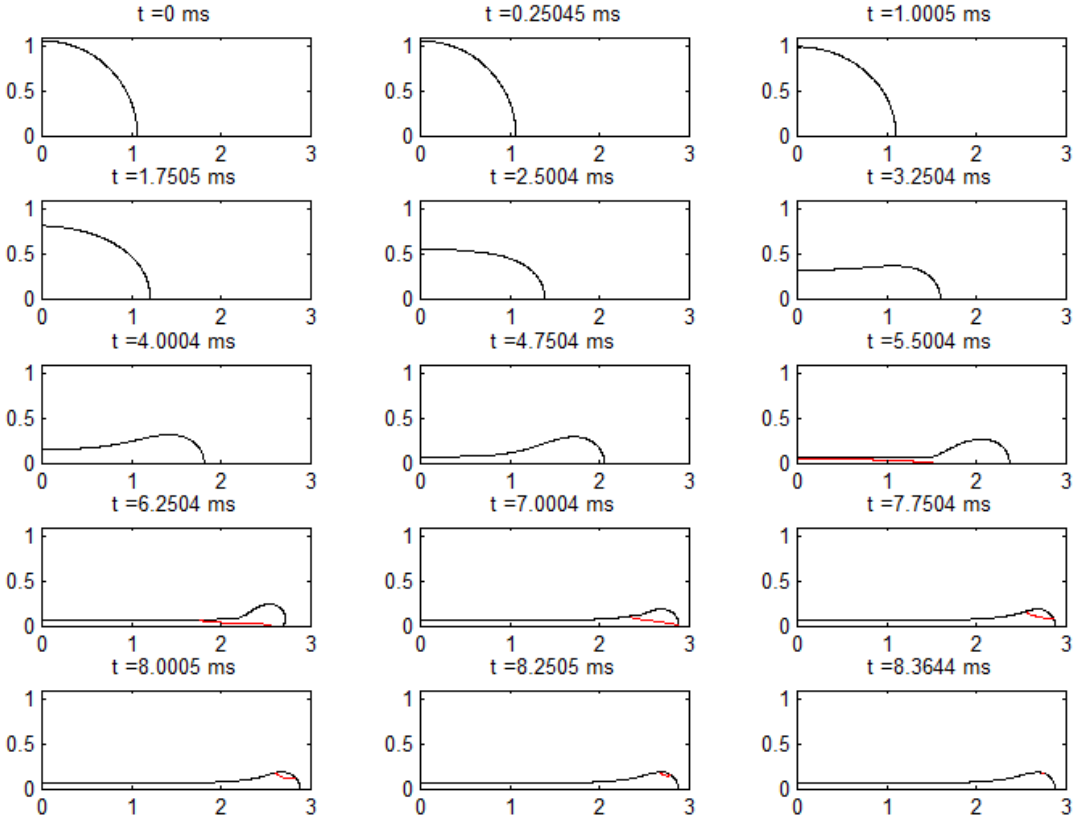

Figure 4.21: Droplet with an initial temperature of 1300 K

4.6.5 Effect of Latent Heat

Latent heat is energy released or absorbed, by a body or a thermodynamic system, during a constant-temperature process. There is no change in the kinetic energy of the particles in the material. It measures change in internal energy that seems hidden from a thermometer. The latent heat is normally expressed as the amount of heat (in units of joules or calories) per mole or unit mass of the substance undergoing a change of state.

In the present study, cases were carried out with different latent heat values varying in steps of $10kJ/kg$ from $30kJ/kg$ to $80kJ/kg$. Droplet spreading for the above mentioned latent heat values is shown below in Figure(4.22). It is seen that due to decrease in the rate of solidification, the spreading increases with increase in latent heat of the droplet implying its influence on the phase change process.

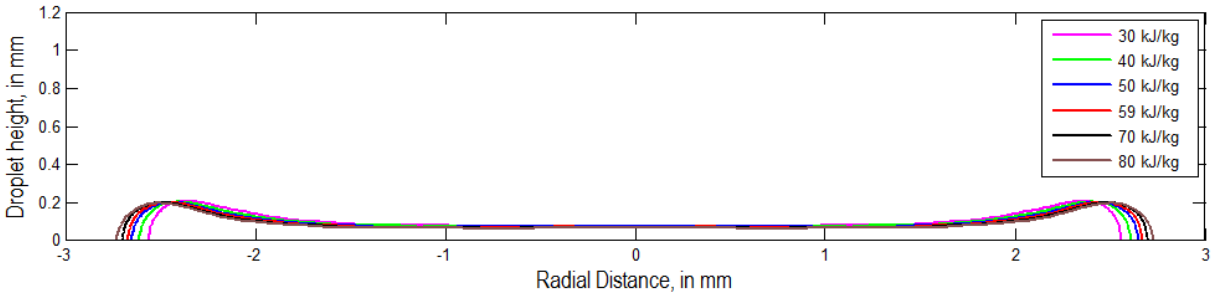

Figure 4.22: Variation of spreading and thickness as a function of latent heat

Solidification time varies in accordance with varying latent heat. In the Figure(4.23) for a value of $30kJ/kg$, spreading is found to be the least in comparison with the other cases. Similarly, in the Figure(4.24) for a latent heat value of $80kJ/kg$, due to larger latent heat spread, this leads to increased solidification time.

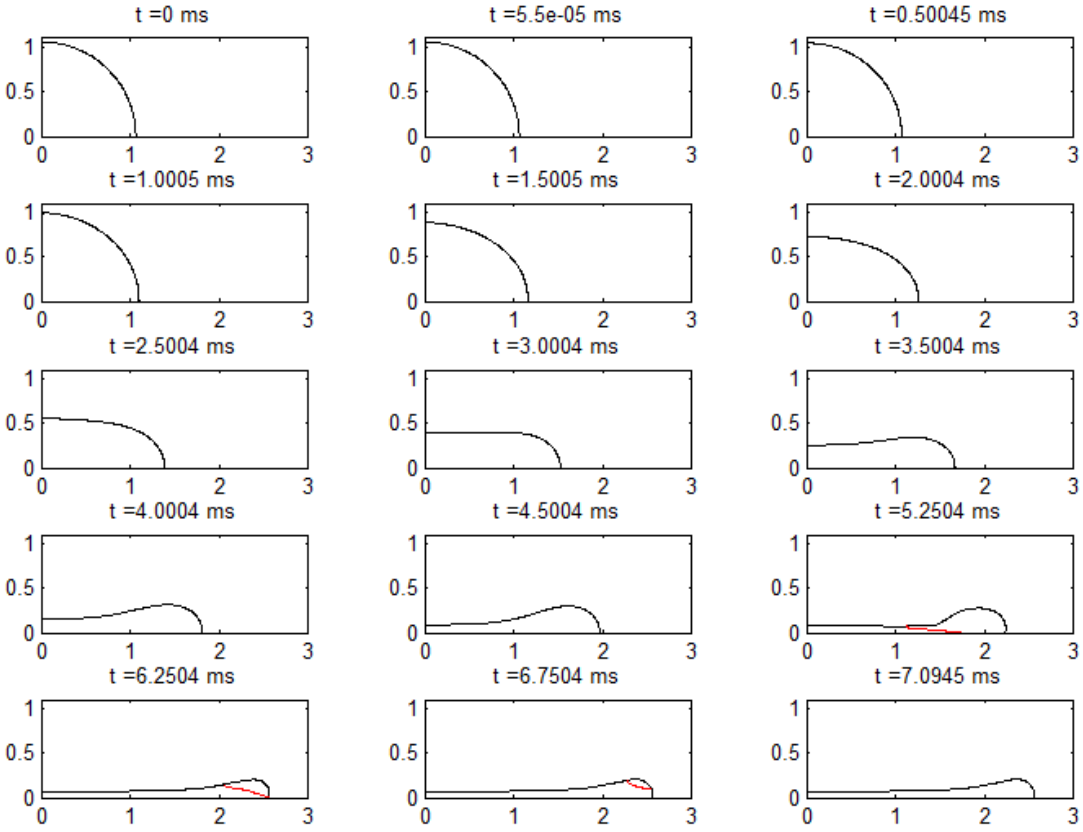

Figure 4.23: 3000 RPM, latent heat value=30 kJ/kg

Stefan number (Ste) is defined as the ratio of sensible heat to latent heat, it is an indicator of rate at which phase change occurs. Varying the value L by holding T_i and T_s constant, a large range of Stefan numbers is obtained. Smaller values of Ste implies more solidification time thereby resulting in larger spreading, whereas larger values of Ste results in shorter solidification time and leads to thicker film and lesser extent of spread It is given by:

$Ste = \frac{SensibleHeat}{LatentHeat} = \frac{C_p(T_i - T_s)}{L}$

where T_i is the initial temperature of the droplet.

T_s is the solidification temperature.

L is the latent heat.

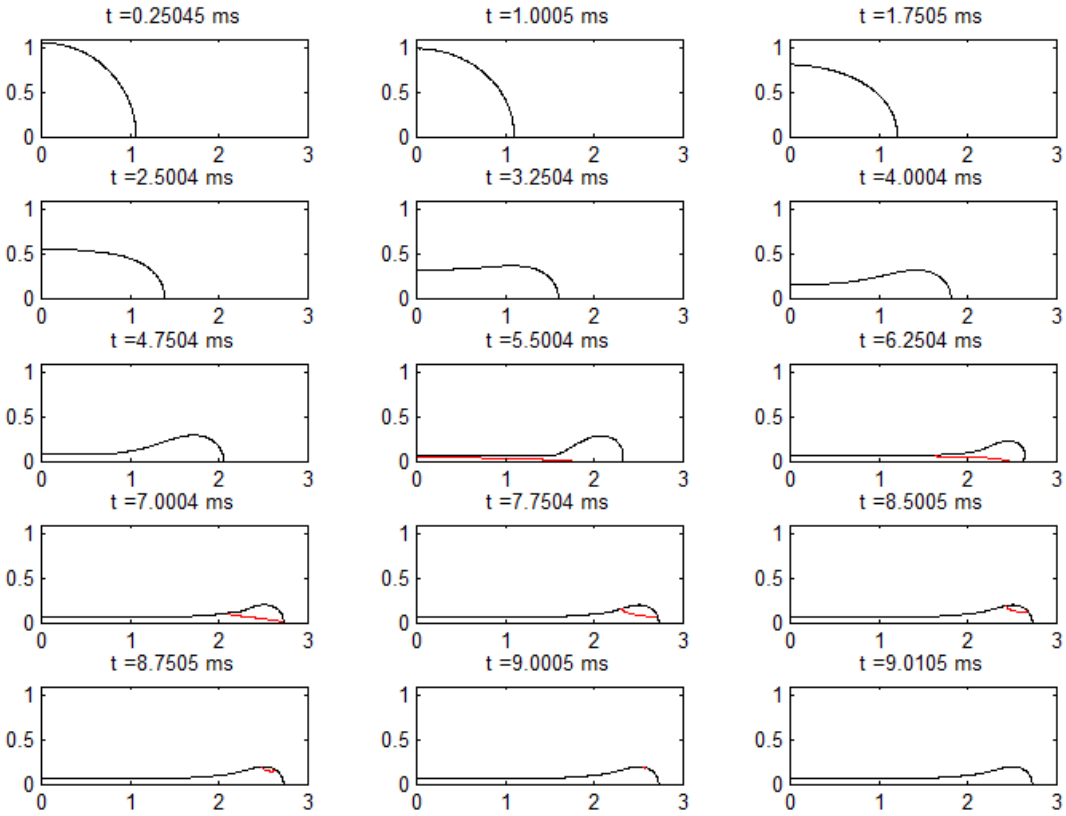

Figure 4.24: 3000 RPM, latent heat value=80 kJ/kg

CHAPTER 5

Conclusion and Future Work

5.1 Conclusion

Spin coating process is incompressible in nature. The analysis of the same is done using modified RIPPLE, a two dimensional incompressible flow solver. The Continuity and the Navier-Stokes equations are solved in conjunction to obtain the velocity and pressure field. Free surface tracking is done using Coupled Level Set Volume of Fluid (CLSVOF) method. Continuum Surface Force (CSF) has been used to calculate surface tension force. Solidification is done using an enthalpy-porosity technique with a source term accounting for phase change.The study was carried out using pure Tin. Centrifugal Force was modeled using a function accounting for the acceleration. The evolution of free surface was in good agreement with the previous study by other researchers.

A grid refinement study was carried out and a square grid with a cell size of 0.01mm was selected for the further case study. Computational domain size was varied according to the angular velocity. A parametric study was carried out. The parameters studied were angular velocity, ramp rate, latent heat, substrate and droplet temperatures.

Effect of angular velocity on the thickness and spread was studied and it was observed that spreading increased with increase in angular velocity leading to thinner film formation. The effect of ramp rate on the spreading and the thickness is very similar to that of effect of angular velocity. A larger ramp rate implied lesser time taken to reach the specified angular velocity, leading to larger spread

and thinner coating being achieved.

The study on effect of substrate temperature showed that lower the substrate temperature lesser is the spread and coating obtained is thicker. As substrate temperature is increased droplet solidification rate decreases allowing for larger spreading. In the study of effect of droplet temperature it is observed that as droplet temperature increases, the spreading and solidification time increases this is due to the more amount of sensible heat that the droplet possesses. Latent heat study is purely numerical in nature, higher the latent heat value, more is time needed for the droplet to solidify. A dimensionless number of importance in the study of phase change process is Stefan number. Stefan number is the ratio of sensible heat to the latent heat. Hence the Stefan number variation can be brought about by varying droplet temperature and/or latent heat. Higher the Stefan number, lower the solidification time and the same has been observed in the study of effects of droplet temperature and latent heat on the solidification process.

The results obtained in this study is well in accordance with the laws of physics governing the process of droplet under the action of centrifugal force and the process of solidification.

5.2 Future Work

Research is a continuous process and there is always scope for improvement. The free surface is considered adiabatic in the code where no heat exchange occurs between the free surface. Suitable work towards incorporating an numerical model for evaporative effects could lead to better understanding of phase change from liquid to gaseous state.

Numerical study based on spin coating can be carried out using non linear/unstructured grid and a parallel can be drawn listing the pros and cons of both structures and unstructured grids. The use of unstructured grids limits us to use only Volume of Fluid (VOF) method, as few sections of Coupled Level Set Volume of Fluid (CLSVOF) method is hard coded to work in conjunction with only structured grids. Generalizing those sections of CLSVOF method could lead to a thorough study based on the nature of grids used.

The present study can be extended to other metals such as Aluminum. Different droplet sizes can be used to study the effect of size on spreading. A larger droplet size would imply weaker effects of surface tension hence allowing more spreading for lower spin speeds. Present study was limited to spreading of the droplet on a substrate without taking into account the thickness of it. A finite thickness substrate will help us in addressing the effects of substrate remelting. Present study was done using a two dimensional flow solver. With the use of three dimensional model, particular cases such as finger formation during the spreading can be studied. In the present study, the droplet was modeled on the substrate as initial setup. Cases can be carried out by modeling droplet at a certain height and effect of impact velocity on the spreading in conjunction with angular velocity

APPENDIX A

Code Execution

A.1 Execution of the Code

The name of the code used for the study is RIPPLE, which has been modified to accommodate heat transfer and phase change and written on FORTRAN. LINUX based high performance computing is used to compile and execute the program. The numerical simulations were carried out on two platforms.

- High Performance Computing, at University of Texas at Arlington
- Lonestar 4 and Lonestar 5 supercomputer clusters at Texas Advanced Computing Center(TACC), Austin,Tx

Four unique files are required to run the code which has been compiled on the supercomputer cluster. They are

- filename.dat
- bjob
- input
- ripple

All the four files are to be placed in the same folder. The filename.dat is a data type of file which contains the number of output files to be generated with the names of files written into it. bjob is a file that provides load sharing facility, generates a job id, places it in the queue that is decided by the number of cores needed for the execution of the case. input file houses information about fluid parameters, mesh size and parameters related to heat transfer. ripple is a executable file which is generated after the code gets compiles successfully. It contains the flow of instructions for it carryout the numerical simulation.

Droplet Spin [mm,ms,mg,K]

$numparam

alpha=1.0,

autot=1.0,

conserve=.false.,

delt=0.5e-4,

dtmax=1.0e-3,

twfin=200000.0,

con = 0.5,

fcvlim=0.5,

idiv=1,

dmpdt=3000000.0,

prtdt=1000000.0,

pltdt=0.25,

sym=.true.,

kt=1,

kb=2,

kl=1,

kr=3,

$end

$fldparam

gy=-9.81e-3,

icyl=1,

isurf10=1,

psat= 0.0,

xnu=1.8e-4,

rhof=6.95,

sigma=0.55,

vi=0.0,

spinvel=0.3158

heif=1.0

$end

$mesh

nkx=1, xl=0.0,4.0,

xc=2.0,

nxl=200,

nxr=200,

dxmn=0.01,

nky=1,

yl=0.0,1.20,

yc=0.6,

nyl=60

nyr=60

dymn=0.01,

$end

$obstcl

nobs=0,

$end

$freesurf

nfrsrf=2,iequib=0,

fc1(1)=-1,ifh(1)=1

fa1(2)=0.0, fa2(2)=1.0, fb1(2)=0.0, fb2(2)=1.0, fc1(2)=-33.64,

ifh(2)=0,

$end

$graphics

plots=.true., dump=.false.,

iout = 0, 0, 0, 0, 0, 0, 0, 0, 0, 0, 0, 0, 0,

0, 0, 0, 0, 0, 0, 0, 0, 0, 0, 0, 0, 0,

0, 0, 0, 0, 0, 0, 0, 2,0,0,-1, 0, 1,

iysymplt=1,

$end

$heateq

heat = .true.,

ischeme = 3,

tid = 1100.0,

tip = 500.0,

tia = 288.0,

cpp = 240.0,

cpd = 240.0,

cpa = 50.0,

tkp = 66.8,

tkd = 66.8,

lhpc = 59000,

hmr = 30.0,

tl = 505.5,

ts = 504.5,

teps = 1.0e-8,

$end

$coupled

lsvof=.true.,

ls=.false.,

$end

Output file

The output files generated over the entire simulation carries unique name. It is of the form *rippxxx.dat*. It contains the information listed below:

- Time at that instant
- Size of the computational domain.
- Location of cells in X and Y direction.
- X and Y components of velocity.
- VOF and LS function values
- Enthalpy and Pressure values pertaining to each cell.

A sample of output file is shown below.

Sample of Output file is shown below.

```
1.00045E+000    Time
 2,560          First real cell in X direction, last real cell in X direction
 2,120          First real cell in Y direction, last real cell in Y direction
0.00000E+000    Location of left side of computationa cell in X direction
1.00000E-002
2.00000E-002
3.00000E-002
............

0.00000E+000    Location of lower side of computationa cell in Y direction
1.00000E-002
2.00000E-002
3.00000E-002
............

1.44400E-002,    -9.85423E-002,    1.00000E+000,   1.00000E+000,   2.39932E+005,   1.15254E-001
1.56472E-002,    -9.85537E-002,    1.00000E+000,   1.00000E+000,   2.39927E+005,   1.17492E-001
1.68552E-002,    -9.85655E-002,    1.00000E+000,   1.00000E+000,   2.39921E+005,   1.19928E-001
1.80642E-002,    -9.85777E-002,    1.00000E+000,   1.00000E+000,   2.39915E+005,   1.22563E-001
1.92741E-002,    -9.85903E-002,    1.00000E+000,   1.00000E+000,   2.39909E+005,   1.25396E-001
2.04850E-002,    -9.86030E-002,    1.00000E+000,   1.00000E+000,   2.39901E+005,   1.28428E-001
Velocity Comp     Velocity Comp    VOF function    LS function     Enthalpy        Pressure
in X direction   in Y direction
```

REFERENCES

[1] A. Y. Tong and Z. Wang, "A numerical method for capillarity-dominant free surface flows," *Journal of Computational Physics*, vol. 221, no. 2, pp. 506–523, 2007.

[2] X. Wu, N. Phan-Thien, X. J. Fan, and T. Y. Ng, "A molecular dynamics study of drop spreading on a solid surface," *Physics of Fluids*, vol. 15, no. 6, pp. 1357–1362, 2003.

[3] A. G. Emslie, F. T. Bonner, and L. G. Peck, "Flow of a viscous liquid on a rotating disk," *Journal of Applied Physics*, vol. 29, no. 5, pp. 858–862, 1958.

[4] D. Meyerhofer, "Characteristics of resist films produced by spinning," *Journal of Applied Physics*, vol. 49, no. 7, pp. 3993–3997, 1978.

[5] N. Sahu, B. Parija, and S. Panigrahi, "Fundamental understanding and modeling of spin coating process: A review," *Indian Journal of Physics*, vol. 83, no. 4, pp. 493–502, 2009.

[6] D. B. Kothe, R. C. Mjolsness, and M. D. Torrey, "RIPPLE: A Computer Program for Incompressible Flows with Free Surfaces," 1994.

[7] Z. Wang and A. Y. Tong, "A sharp surface tension modeling method for two-phase incompressible interfacial flows," *International Journal for Numerical Methods in Fluids*, vol. 64, no. 7, pp. 709–732, 2010.

[8] Z. Wang, "Numerical study on capillarity-dominant free surface and interfacial flows," *Mechanical Engineering*, no. May, p. 156, 2006.

[9] D. S. Kershaw, "The incomplete cholesky conjugate gradient method for the iterative solution of systems of linear equations," *Journal of Computational Physics*, vol. 26, no. 1, pp. 43–65, 1978.

[10] E. Maitre, "Review of numerical methods for free interfaces," *Les Houches*, pp. 27–31, 2006.

[11] F. H. Harlow, J. E. Welch, *et al.*, "Numerical calculation of time-dependent viscous incompressible flow of fluid with free surface," *Physics of fluids*, vol. 8, no. 12, p. 2182, 1965.

[12] C. Hirt and B. Nichols, "Volume of fluid (VOF) method for the dynamics of free boundaries," *Journal of Computational Physics*, vol. 39, no. 1, pp. 201–225, 1981.

[13] J. A. Sethian, "Theory, algorithms, and applications of level set methods for propagating interfaces," *Acta numerica*, vol. 5, pp. 309–395, 1996.

[14] S. Osher and R. Fedkiw, *Level set methods and dynamic implicit surfaces*. Springer Science & Business Media, 2006, vol. 153.

[15] M. Sussman and E. Fatemi, "An efficient, interface-preserving level set redistancing algorithm and its application to interfacial incompressible fluid flow," *SIAM Journal on scientific computing*, vol. 20, no. 4, pp. 1165–1191, 1999.

[16] G. Son and N. Hur, "A coupled level set and volume-of-fluid method for the buoyancy-driven motion of fluid particles," *Numerical Heat Transfer: Part B: Fundamentals*, vol. 42, no. 6, pp. 523–542, 2002.

[17] M. Rudman, "Volume-tracking methods for interfacial flow calculations," *International journal for numerical methods in fluids*, vol. 24, no. 7, pp. 671–691, 1997.

[18] F. Moulin and J.-B. Flór, "On the spin-up by a rotating disk in a rotating stratified fluid," *Journal of Fluid Mechanics*, vol. 516, pp. 155–180, 2004.

[19] A. Y. Tong and B. R. Holt, "Numerical study on the solidification of liquid metal droplets impacting onto a substrate," *Numerical Heat Transfer, Part A Applications*, vol. 31, no. 8, pp. 797–817, 1997.

[20] S. Patankar, *Numerical heat transfer and fluid flow.* CRC Press, 1980.

[21] D.E. Bornside, C. W. Macosko and L. E. Scriven, "Spin Coating of a PMMA/Chlorobenzene Solution."

[22] E. Cueto, a. W. K. Ma, F. Chinesta, and M. R. Mackley, "Numerical simulation of spin coating processes involving functionalised Carbon nanotube suspensions," *International Journal of Material Forming*, vol. 1, no. 2, pp. 89–99, 2008.

[23] R. H. Chen and C. M. Cheng, "Study of Spin Coating Properties of SU-8 Thick-layer Photoresist," *Advances in Resist Technology and Processing XVIII*, vol. 4345, no. 2001, pp. 494–501, 2001.

[24] Y. Gu, "A model for a liquid drop spreading on a solid surface," *Colloids and Surfaces A: Physicochemical and Engineering Aspects*, vol. 142, no. 2-3, pp. 243–256, 1998.

[25] D. Riendeau, "Circular motion," *The Physics Teacher*, vol. 50, no. 1, p. 58, 2012.

[26] W. W. Flack, D. S. Soong, A. T. Bell, and D. W. Hess, "Mathematical Model for Spin Coating of Polymer Resists." *Journal of Applied Physics*, vol. 56, no. 4, pp. 1199–1206, 1984.

[27] J. Y. Jung, Y. T. Kang, and J. Koo, "Development of a new simulation model of spin coating process and its application to optimize the 450 mm wafer coating process," *International Journal of Heat and Mass Transfer*, vol. 53, no. 9-10, pp. 1712–1717, 2010.

[28] S. Sharafat and N. Ghoniem, "Summary of Thermo-Physical Properties of Sn , Comparison of Properties of Sn , Sn-Li , Li , and Pb-Li," *UCLA-UCMEP-00-31 Report*, pp. 1–51, 2000.

[29] L. W. Schwartz and R. V. Roy, "Theoretical and numerical results for spin coating of viscous liquids," *Physics of Fluids*, vol. 16, no. 3, pp. 569–584, 2004.

[30] D. E. Bornside, C. W. Macosko, and L. E. Scriven, "Spin coating: One-dimensional model," *Journal of Applied Physics*, vol. 66, no. 11, pp. 5185–5193, 1989.

[31] D. B. Hall, P. Underhill, and J. M. Torkelson, "Spin Coating of Thin and Ultrathin Polymer Films," *Polymer Engineering and Science*, vol. 38, no. 12, pp. 2039–2045, 1998.

[32] R. K. Yonkoski and D. S. Soane, "Model for spin coating in microelectronic applications," *Journal of Applied Physics*, vol. 72, no. 2, p. 725, 1992.

[33] Wikipedia, "Contact Angle," pp. 2–5, 2015.

[34] D. P. Birnie III, S. K. Hau, D. S. Kamber, and D. M. Kaz, "Effect of ramping-up rate on film thickness for spin-on processing," *Journal of Materials Science: Materials in Electronics*, vol. 16, no. 11-12, pp. 715–720, 2005.